




## RESEARCH ARTICLE

# A novel mouse model of diffuse midline glioma initiated in neonatal oligodendrocyte progenitor cells highlights cell-of-origin dependent effects of H3K27M

Yusuke Tomita<sup>1,2</sup>  | Yosuke Shimazu<sup>1</sup>  | Agila Somasundaram<sup>3</sup> |  
Yoshihiro Tanaka<sup>4,5</sup> | Nozomu Takata<sup>6,7</sup> | Yukitomo Ishi<sup>1</sup> | Samantha Gadd<sup>8</sup> |  
Rintaro Hashizume<sup>1,3,9</sup> | Angelo Angione<sup>10</sup> | Gonzalo Pinero<sup>10</sup> |  
Dolores Hambarzumyan<sup>10</sup> | Daniel J. Brat<sup>11</sup> | Christine M. Hoeman<sup>1</sup> |  
Oren J. Becher<sup>1,3,9,12</sup> 

<sup>1</sup>Department of Pediatrics, Feinberg School of Medicine, Northwestern University, Chicago, Illinois, USA

<sup>2</sup>Department of Neurosurgery and Neuroendovascular Surgery, Hiroshima City Hiroshima Citizens Hospital, Hiroshima, Japan

<sup>3</sup>Division of Hematology, Oncology and Stem Cell Transplant, Ann & Robert H. Lurie Children's Hospital of Chicago, Chicago, Illinois, USA

<sup>4</sup>Department of Preventive Medicine, Northwestern University Feinberg School of Medicine, Chicago, Illinois, USA

<sup>5</sup>Center for Arrhythmia Research, Department of Cardiology, Northwestern University Feinberg School of Medicine, Chicago, Illinois, USA

<sup>6</sup>Center for Vascular and Developmental Biology, Feinberg Cardiovascular and Renal Research Institute (FCVRR), Northwestern University, Chicago, Illinois, USA

<sup>7</sup>Simpson Querrey Institute for BioNanotechnology, Northwestern University, Chicago, Illinois, USA

<sup>8</sup>Department of Pathology, Ann & Robert H. Lurie Children's Hospital of Chicago, Chicago, Illinois, USA

<sup>9</sup>Department of Biochemistry and Molecular Genetics, Feinberg School of Medicine, Northwestern University, Chicago, Illinois, USA

<sup>10</sup>Department of Neurosurgery and Oncological Sciences, Mount Sinai School of Medicine, New York, USA

<sup>11</sup>Department of Pathology, Feinberg School of Medicine, Northwestern University, Chicago, Illinois, USA

<sup>12</sup>Jack Martin Division of Pediatric Hematology-oncology, Mount Sinai Kravis Children's Hospital, New York, USA

## Correspondence

Oren J. Becher, Department of Pediatrics, Feinberg School of Medicine, Northwestern University, Chicago, IL, USA.  
Email: [oren.becher@gmail.com](mailto:oren.becher@gmail.com); [oren.becher@mssm.edu](mailto:oren.becher@mssm.edu)

## Funding information

Foundation for the National Institutes of Health, Grant/Award Numbers: K02 NS086917, R01 CA197313, R21 1R21NS114431-01

## Abstract

Diffuse midline glioma (DMG) is a type of lethal brain tumor that develops mainly in children. The majority of DMG harbor the K27M mutation in histone H3. Oligodendrocyte progenitor cells (OPCs) in the brainstem are candidate cells-of-origin for DMG, yet there is no genetically engineered mouse model of DMG initiated in OPCs. Here, we used the RCAS/Tv-a avian retroviral system to generate DMG in Olig2-expressing progenitors and Nestin-expressing progenitors in the neonatal mouse brainstem. PDGF-A or PDGF-B overexpression, along with p53 deletion,

**Abbreviations:** CFP, cyan fluorescent protein; DAPI, 4',6-diamidino-2-phenylindole; DIPG, diffuse intrinsic pontine glioma; DMG, diffuse midline glioma; EMT, epithelial-to-mesenchymal transition; EZH2, enhancer of zeste homolog 2; Gata3, GATA binding protein 3; GEMM, genetically engineered mouse model; GFP, green fluorescent protein; GSEA, gene set enrichment analysis; H&E, hematoxylin and eosin; IHC, immunohistochemistry; Lhx5, LIM homeobox protein 5; Lmx1b, LIM homeobox transcription factor 1 beta; NPC, neural progenitor cell; Ntv-a, Nestin-Tv-a; OPC, oligodendrocyte progenitor cell; Otv-a, Olig2-Tv-a; PBS, phosphate-buffered saline; PDGF, platelet-derived growth factor; Phox2b, paired-like homeobox 2b; PRC2, polycomb repressive complex 2; TNFA, tissue necrosis factor-alpha; TP53, tumor protein 53; WT, wild type.

Yusuke Tomita and Yosuke Shimazu contributed equally to this work.

This is an open access article under the terms of the [Creative Commons Attribution-NonCommercial-NoDerivs](https://creativecommons.org/licenses/by-nc-nd/4.0/) License, which permits use and distribution in any medium, provided the original work is properly cited, the use is non-commercial and no modifications or adaptations are made.

© 2022 The Authors. GLIA published by Wiley Periodicals LLC.



resulted in gliomas in both models. Exogenous overexpression of H3.3K27M had a significant effect on tumor latency and tumor cell proliferation when compared with H3.3WT in Nestin<sup>+</sup> cells but not in Olig2<sup>+</sup> cells. Further, the fraction of H3.3K27M-positive cells was significantly lower in DMGs initiated in Olig2<sup>+</sup> cells relative to Nestin<sup>+</sup> cells, both in PDGF-A and PDGF-B-driven models, suggesting that the requirement for H3.3K27M is reduced when tumorigenesis is initiated in Olig2<sup>+</sup> cells. RNA-sequencing analysis revealed that the differentially expressed genes in H3.3K27M tumors were non-overlapping between Olig2;PDGF-B, Olig2;PDGF-A, and Nestin;PDGF-A models. GSEA analysis of PDGFA tumors confirmed that the transcriptomal effects of H3.3K27M are cell-of-origin dependent with H3.3K27M promoting epithelial-to-mesenchymal transition (EMT) and angiogenesis when Olig2 marks the cell-of-origin and inhibiting EMT and angiogenesis when Nestin marks the cell-of-origin. We did observe some overlap with H3.3K27M promoting negative enrichment of TNFA\_Signaling\_Via\_NFKB in both models. Our study suggests that the tumorigenic effects of H3.3K27M are cell-of-origin dependent, with H3.3K27M being more oncogenic in Nestin<sup>+</sup> cells than Olig2<sup>+</sup> cells.

**KEYWORDS**

diffuse intrinsic pontine glioma, diffuse midline glioma, H3K27M, oligodendrocyte progenitor cells

## 1 | INTRODUCTION

Diffuse midline glioma (DMG) accounts for 15%–20% of pediatric brain tumors and represents the leading cause of death in children with brain tumors (Buczakowicz & Hawkins, 2015). The critical location and diffuse nature of the tumor precludes surgical resection, and radiotherapy offers only transient symptomatic relief. Despite numerous clinical trials, no chemotherapy approach has prolonged the survival of children with DMG. The failure of these trials is partly due to the adaptation of established treatments for adult glioma, which have been evaluated in adult patients, for children (Hargrave et al., 2006).

Approximately 85% of DMG contain the somatic gain-of-function K27M mutation in histones H3.1 and H3.3 but these mutations are extremely rare in adult gliomas (Bender et al., 2013; Chan et al., 2013; Schwartzenuber et al., 2012; Wu et al., 2012). Nearly 60% of the K27M mutations in DMG involve a single allele in H3F3A encoding H3.3 (Schwartzenuber et al., 2012). H3K27M mutations are thought to drive DMG formation (Chan et al., 2013; Schwartzenuber et al., 2012; Wu et al., 2012). The H3K27M mutation reduces global histone H3K27 methylation (H3K27me<sub>3</sub>) by inhibiting polycomb repressive complex 2 (PRC2) activity (Lewis et al., 2013). As H3K27me<sub>3</sub> primarily correlates with gene repression, H3K27M mutations result in a net gain in cellular transcriptional activity (Chan et al., 2013; Funato et al., 2014; Lewis et al., 2013). However, for certain genes such as the tumor suppressor p16 or Ink4a, associated H3K27me<sub>3</sub> is retained or even increased in some experimental models resulting in increased gene repression (Bender et al., 2013;

Brien et al., 2021; Cordero et al., 2017; Mohammad et al., 2017). Thus, the mutation's effects on H3K27 methylation and gene expression are aimed at a combination of gene activation and suppression that collectively promote tumor growth.

Others and we have previously shown that the oncogenic properties of the H3.3K27M mutation are dependent on the glioma cell-of-origin. For example, in Nestin<sup>+</sup> neural progenitor cells (NPCs), H3.3K27M combined with platelet-derived growth factor B (PDGF-B) expression and p53 loss induces DMG, alters gene-expression, and reduces the survival of tumor-bearing mice (Cordero et al., 2017; Lewis et al., 2013). But an effect on tumor latency is not seen with Pax3<sup>+</sup> cells, which include neurons and undifferentiated progenitors (Misuraca et al., 2016). Further, H3.3K27M increases the proliferation of neural stem cells derived from human embryonic stem cells, but not so for early astrocytes (Funato et al., 2014). Recent studies have implicated oligodendrocyte progenitor cells (OPCs) of the neonatal brainstem as the likely cell-of-origin for DMG (Filbin et al., 2018; Lindquist et al., 2016; Nagaraja et al., 2017; Tate et al., 2015), consistent with prior studies showing a spatiotemporal correlation between Olig2<sup>+</sup> precursor proliferation in human and mouse brainstem and brainstem glioma occurrence in children (Monje et al., 2011). Single cell RNA-sequencing (RNA-seq) analysis has revealed that the majority of the cells in H3K27M gliomas express OPC-like transcriptomes (Filbin et al., 2018). The most active promoter enhancers in H3.3K27M tumor cells are associated with genes of the oligodendroglial lineage (Nagaraja et al., 2017), and OPCs are the most proliferative precursor cell-type in the neonatal ventral pons, coinciding

spatiotemporally with the development of midline gliomas (Lindquist et al., 2016). Despite these findings, the characteristics of H3.3K27M-bearing diffuse gliomas initiated in OPCs are not known.

Here, we describe a novel genetically engineered mouse model (GEMM) of diffuse intrinsic pontine glioma (DIPG, a subset of DMG that occurs in the pons) initiated in neonatal Olig2<sup>+</sup> progenitors. We used the RCAS/Tv-a avian retroviral system to introduce gene alterations that are commonly found in human DIPG (H3.3K27M, PDGF-B, or PDGF-A to activate PDGFRA signaling, and p53 inactivation) (Khuong-Quang et al., 2012; Mackay et al., 2017; Wu et al., 2012) in Olig2<sup>+</sup> progenitors. The resulting diffuse midline high grade gliomas exhibited histological and immunophenotypical characteristics such as infiltration and leptomeningeal dissemination that closely resemble the human disease. Surprisingly, H3.3K27M expression had only a minor effect on tumor latency and no significant effect on proliferation relative to H3.3WT tumors, in contrast with H3K27M tumors originating in Nestin<sup>+</sup> cells. GSEA analysis revealed that H3.3K27M has cell-of-origin dependent effects on key gene-sets with known roles in tumorigenesis. For example, H3.3K27M mutant tumors were significantly positively enriched for EMT and angiogenesis when Olig2 marks the cell-of-origin but H3.3K27M tumors were negatively enriched for angiogenesis and EMT when nestin marked the cell-of-origin. Thus, our study provides a novel DIPG mouse model initiated in Olig2<sup>+</sup> OPCs that can be used for mechanistic studies and preclinical evaluation of novel therapies for DIPG. Our results highlight cell-of-origin dependent effects of H3.3K27M with a more oncogenic role for H3K27M in Nestin<sup>+</sup> cells relative to Olig2<sup>+</sup> cells.

## 2 | MATERIALS AND METHODS

### 2.1 | Mice

Olig2-Tv-a-Cre (Otv-a-Cre) mice were obtained from Jackson Labs. The genomic structure and characteristics of these mice have been previously reported (Schüller et al., 2008). Otv-a-Cre mice were intercrossed with conditional null p53 mice (Jackson Labs, C57BL/6J background) to generate Otv-a-Cre;p53<sup>fl/fl</sup> and Otv-a-Cre;p53<sup>fl/+</sup> mice, as previously described (Mehta et al., 2011). Nestin-Tv-a;p53<sup>fl/fl</sup> (Ntv-a;p53<sup>fl/fl</sup>) mice were created by crossing Ntv-a and p53<sup>fl/fl</sup> mice (Barton et al., 2013). Nestin-CFPnuc mice express cyan fluorescent protein (CFP) fused to a nuclear localization signal under the control of the Nestin enhancer (Encinas et al., 2006; Misuraca et al., 2016). All animals were maintained in accordance with the Northwestern University Animal Care and Use Committee guidelines (animal protocol IS00012699).

### 2.2 | Generation of in vivo murine midline gliomas

In vivo midline gliomas were generated using the RCAS/Tv-a system as previously described (Misuraca et al., 2014; Misuraca et al., 2016). DF1 cells were purchased from American Type Culture Collection

(Manassas) and were grown in Dulbecco's Modified Eagle Medium, supplemented with 10% fetal bovine serum, 2 mm/L L-glutamine, 100 U/ml penicillin, and 100 mg/ml streptomycin, at 39°C and 5% CO<sub>2</sub>. Cells were transfected with RCAS plasmids (RCAS-PDGF-A, RCAS-PDGF-B, RCAS-H3.3WT-GFP, RCAS-H3.3K27M-GFP, RCAS-Cre). Postnatal day 3 to 5 (P3-P5) mice were injected intracranially with 1  $\mu$ l of RCAS virus producing DF1 cells (10<sup>5</sup> cells). Injected mice were monitored daily and euthanized with CO<sub>2</sub> upon the appearance of brain tumor symptoms (enlarged head, ataxia, weight loss up to 25%) or at 6 months postinjection in the absence of symptoms.

### 2.3 | Immunofluorescence

Nestin-CFPnuc mice were euthanized at P3, brains were extracted and fixed in 4% paraformaldehyde in phosphate-buffered saline (PBS) for 24 h and cryopreserved in 30% sucrose in PBS for 24–48 h. After embedding in OCT compound, blocks were sectioned using a Cryostat (TN50, Tanner Scientific, Inc.) into 10  $\mu$ m thick sagittal or oblique coronal sections to visualize the whole pons (Lindquist et al., 2016). Sections were rehydrated in PBS with 0.1% Triton X-100 (PBS-T). Antigen retrieval was performed using citrate buffer pH 6 for 20 min at 95°C. Sections were then permeabilized using PBS-T with 0.3% Triton X-100 and blocked with PBS-T containing 5% normal donkey serum. Anti-Olig2 (Millipore, #AB9610, 1:500), anti-Sox2 (Abcam, ab79351, 1:200), and anti-GFP (Nacalai, 4404-84, 1:1000, to label CFP) primary antibodies were used. AlexaFluor donkey anti-rabbit-488 (Invitrogen, A21208, 1:400), donkey anti-mouse-594 (Invitrogen, A31570, 1:400) and goat anti-rabbit-647 (Invitrogen, A21245, 1:400) were used as secondary antibodies. Slides were mounted with Vectashield with 4',6-diamidino-2-phenylindole (DAPI) (Vector Laboratories) and imaged using a Lionheart™ automated microscope (BioTek, Vermont). The percentages of Nestin-CFP<sup>+</sup>, Olig2<sup>+</sup>, and double-positive cells were quantified with Fiji software (NIH).

### 2.4 | Tumor grading

Tumor tissue was harvested, fixed in 20% formalin for 24–48 h, and embedded in paraffin by the Northwestern University Mouse Histology and Phenotyping Laboratory. Embedded tissue was cut into 5  $\mu$ m sections using a Leica RM2235 microtome. Hematoxylin and eosin (H&E) staining was performed using standard protocols. Tumors were graded by a blinded neuropathologist using the following criteria according to the WHO classification 2016 (Louis et al., 2016): Grade II glioma by moderately increased cellular density without mitosis; Grade III glioma by increased cellular density with mitosis; and Grade IV glioma by the presence of microvascular proliferation and/or pseudopalisading necrosis. WHO Grade III and IV tumors were defined as high-grade. Tumor dissemination was defined as tumor aggregation, existing separately from the main tumor mass (Wagner et al., 2006), in the subependymal spaces of the lateral ventricle or the subcortical space.



## 2.5 | Immunohistochemistry

Mouse tumor tissue sections were prepared as described above. The sections were stained using the Ventana automated system per manufacturer's instruction. Immunohistochemistry (IHC) analyses were carried out as described previously (Hoeman et al., 2019). Anti-GFAP (DAKO, anti-rabbit IgG, #Z0334, 1:2000), anti-GFP (Abcam, anti-rabbit IgG, ab290, 1:1000), anti-H3K27M (Abcam, anti-rabbit IgG, ab190631, 1:500), anti-H3K27me3 (Cell Signaling Technology, anti-rabbit IgG, #9733, 1:200), anti-phospho-Histone H3 (Ser10) (pH3Ser10, Cell Signaling Technology, #97015, 1:200), anti-Iba1 (Wako, #019-19741, 1:500), anti-Ki67 (Abcam, anti-rabbit IgG, ab16667, 1:200), anti-Olig2 (Millipore, anti-rabbit IgG, #AB9610, 1:500), and anti-Nestin (BD Pharmingen, anti-Rat IgG1, #556309, 1:200) were used. Samples were imaged with Zeiss Axio imager, and quantified with Lionheart™ automated microscope and Gen5 software.

## 2.6 | RNA-sequencing and analysis

RNA-sequencing (RNA-seq) and analysis were performed in collaboration with the NUSeq Core facility at Northwestern University. Total RNA was isolated from tumor tissue with the RNeasy Mini Kit (Qiagen), and 200 ng of purified RNA per sample was used for analysis. The libraries were prepared with TruSeq Stranded mRNA-seq Library Prep kit, and sequenced using the HiSeq 4000 sequencing system (Illumina). FASTQ files were aligned to the mm10 genome using RNA-STAR, and aligned reads were counted using HTSeq-count. HTSeq-count files were imported into R (<https://www.r-project.org/>) and differential expression analysis was performed with the DESeq2 package using default settings. H3.3 wild type (WT) was compared to H3.3K27M mutant samples in the presence of PDGF-B or PDGF-A overexpression and p53 deletion. Principal component analysis and hierarchical clustering were done in R. Normalized reads were imported into gene set enrichment analysis (GSEA) and standard GSEA was run with the following parameters: permutations = 1000, permutation type = gene set, enrichment statistic = weighted, gene ranking metric = signal2noise, max size = 500, min size = 15, normalization mode = meandiv. The data discussed in this publication have been deposited in NCBI's Gene Expression Omnibus (GEO, <http://www.ncbi.nlm.nih.gov/geo/>) and are accessible through GEO Series accession number GSE184934, GSE184935, and GSE184936. The number of reads per sample ranged from 23,010,479 to 87,187,138 is listed in Table S1.

## 2.7 | Quantitative real-time PCR (qRT-PCR) analysis

Total RNA was isolated using RNeasy kit (Qiagen) and cDNA synthesized using Superscript IV and OligodT primers (Invitrogen) per manufacturers' instructions. Real-time detection and quantification of cDNA were performed with the QuantiStudio™ 6 Flex kit (Applied Biosystems, #4485691). qRT-PCR was done using Power SYBR Green

qPCR Master mix (Applied Biosystems, #4367659). Gene expression levels were normalized to that of endogenous beta-actin. All experiments were done in triplicates, and relative gene expression levels calculated using the  $\Delta\Delta Ct$  method. Primer sequences are listed in Table S2.

## 2.8 | Statistical analysis

Statistical analysis was performed using GraphPad Prism (Version 9.1.0) for all data. Survival rate was estimated using Kaplan Meier Curve analysis and a statistical significance was evaluated by log-rank test. Continuous variables are expressed as mean  $\pm$  standard deviation (SD) or median (interquartile range: IQR). Categorical variables are expressed as n (%). Continuous variables were compared using Mann-Whitney *U* test, Student's *t* test, or one way ANOVA with Tukey's post hoc test. Categorical variables were compared using Fisher's exact tests.

## 3 | RESULTS

### 3.1 | The majority of Olig2+ in the neonatal brainstem co-express Sox2

We have previously described H3.3K27M glioma initiated in Nestin+ cells in the murine ventral pons (Cordero et al., 2017). Several studies, however, suggest that DIPG likely originates from Olig2+ cells with OPC-like features (Anderson et al., 2017; Filbin et al., 2018). As cell clusters with OPC-like features express both Nestin and Olig2 (Walker et al., 2010), we first evaluated the expression patterns of Olig2 and Nestin, and the extent of overlap of these markers, in the developing mouse brainstem. We immunolabeled sagittal and oblique brain sections (Lindquist et al., 2016) isolated from P3 Nestin-CFPnuc mice with Olig2, Sox2, and GFP antibodies (Figure 1a-l). Distinct clusters of cells immunoreactive for Nestin were found in the ventral and dorsal pons (Figure 1a,d,g,j). Interestingly, majority of the Olig2+ cells co-expressed Sox2 (Figure 1b,e,h,k) and were Nestin negative (Figure 1c,f,i,l). Quantification revealed that over 65% of Olig2+ cells were positive for Sox2 but negative for Nestin (Figure 1m,n). As the study by Lindquist et al. (2016) used the canonical OPC markers SOX10 and PDGFRA to show that the majority of Sox2 + Olig2+ proliferating cells in the P4 pons are OPCs (Lindquist et al., 2016), our results suggest that the RCAS viral infections into the neonatal brainstem at P3-P4 are mainly targeting OPCs.

### 3.2 | H3.3K27M and PDGF-B overexpression in neonatal Olig2+ cells induce midline high grade gliomas

We have previously shown that H3.3K27M and PDGF-B overexpression, along with p53 inactivation, in Nestin+ and Pax3+

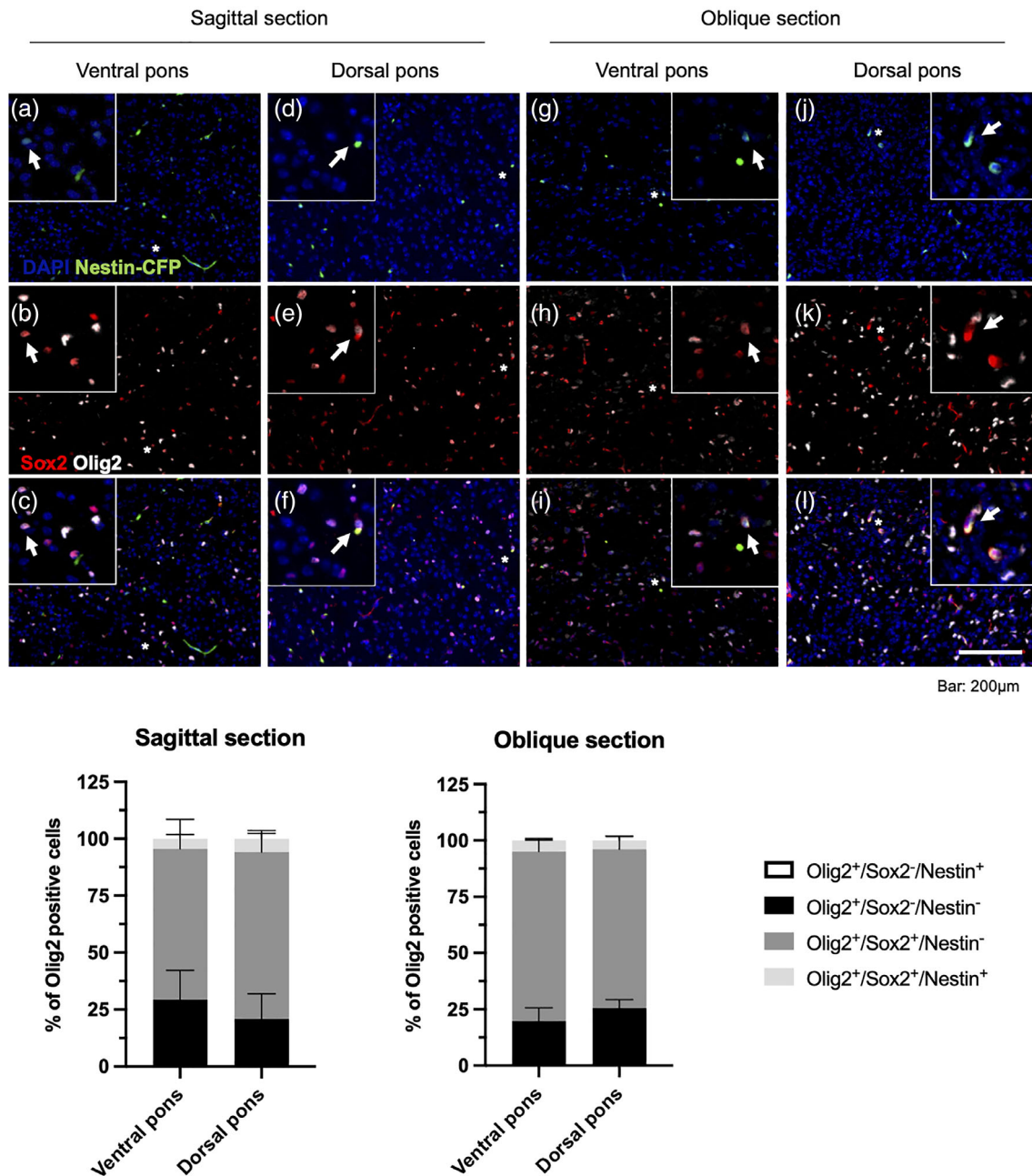


**FIGURE 1** Olig2, Sox2, and nestin expression in the neonatal mouse pons. (a–h) Representative images of P3 mouse ventral (a–c, g–i) and dorsal (d–f, j–l) sagittal and oblique sections of the pons labeled with GFP (green, to visualize Nestin-CFP), Sox2 (red), and Olig2 (white) antibodies. Images were acquired at  $\times 10$  magnification. Scale bars represent 200  $\mu\text{m}$ . Insets show magnified views of the areas marked by asterisks. (m, n) quantification of Olig2<sup>+</sup>/Sox2<sup>-</sup>/Nestin<sup>-</sup>, Olig2<sup>+</sup>/Sox2<sup>+</sup>/Nestin<sup>-</sup>, Olig2<sup>+</sup>/Sox2<sup>-</sup>/Nestin<sup>+</sup>, and Olig2<sup>+</sup>/Sox2<sup>+</sup>/Nestin<sup>+</sup> relative to all Olig2<sup>+</sup> cells in sagittal (m) and oblique (n) section. Mean  $\pm$  SEM,  $n = 3$ –4

progenitors leads to high grade gliomas and increases tumor grade and proliferation relative to H3.3WT when Nestin<sup>+</sup> cells are the cells-of-origin (Barton et al., 2013; Becher et al., 2010; Misuraca et al., 2016). To investigate whether midline gliomas can be initiated in OPCs, we targeted neonatal Olig2<sup>+</sup> cells in Otv-a-Cre mice that express Tv-a and Cre recombinase under the Olig2 promoter (Schüller et al., 2008). Injecting P3–P5 Otv-a-Cre;p53<sup>fl/fl</sup> mice with RCAS-H3.3K27M-GFP did not produce tumor-related symptoms even at 6 months postinfection (Figure S1). When we overexpressed PDGF-B,

however, 100% of infected mice developed neurological symptoms and gliomas regardless of p53 and H3.3K27 status. Otv-a-Cre;p53<sup>fl/fl</sup> mice injected with PDGF-B reached experimental endpoints between 24 and 71 days, Otv-a-Cre;p53<sup>fl/fl</sup> between 48 and 180 days, and Otv-a-Cre mice between 59 and 180 days (Figure 2a–c). Otv-a-Cre;p53<sup>fl/fl</sup> mice overexpressing PDGF-B and H3.3K27M had significantly shorter survival than mice overexpressing PDGF-B and H3.3WT, although the difference was small (Figure 2a, median survival, H3.3K27M, 31 days, H3.3WT, 37 days,  $p = .0473$ , log-rank test).



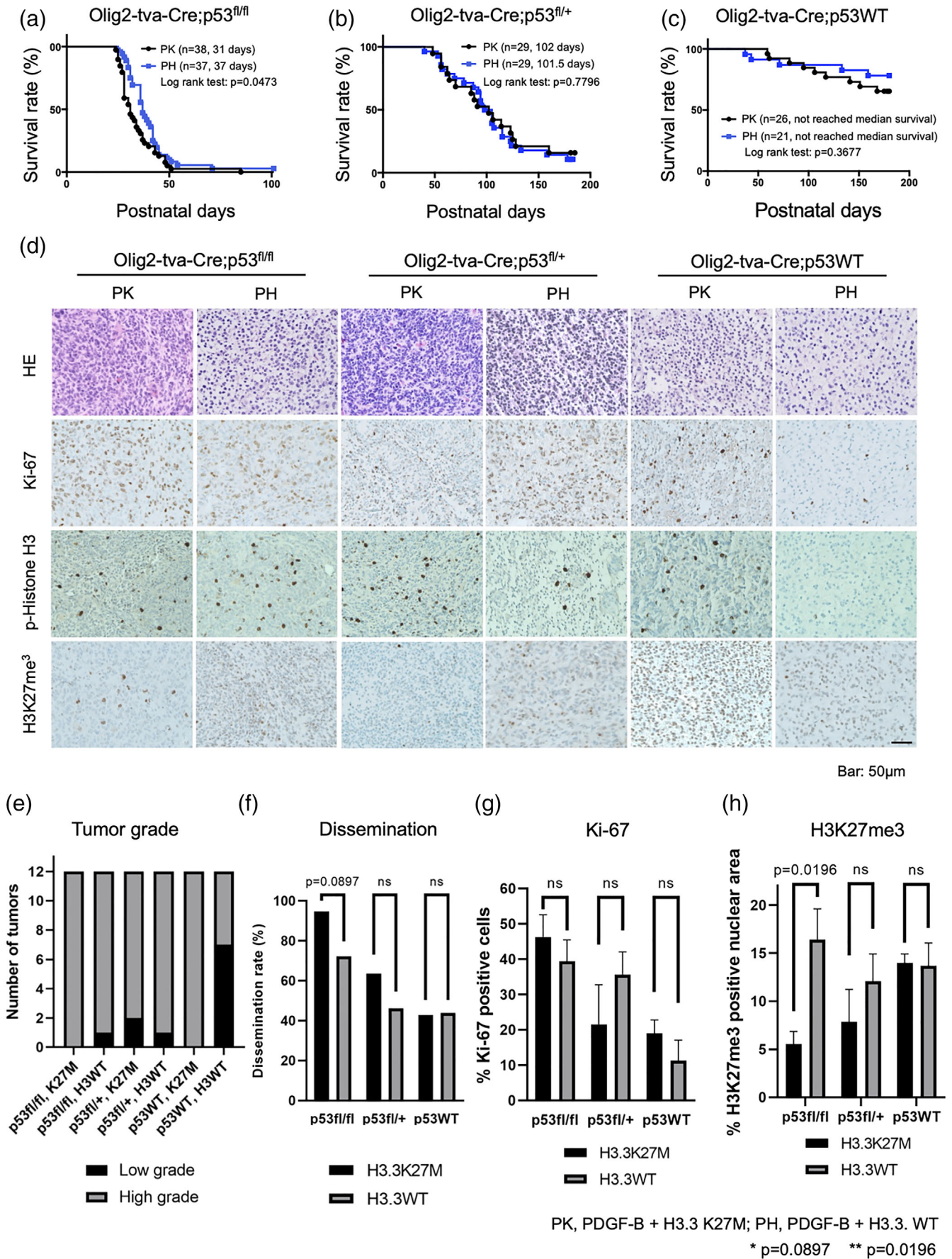


FIGURE 2 Legend on next page.

However, when we performed cox hazard regression analysis, the male sex but not H3.3K27 status was an independent poor prognostic factor (Table S3). No significant difference in survival was seen between H3.3K27M and H3.3WT infected Otv-a-Cre; p53<sup>fl/+</sup> mice (Figure 2b, median survival, H3.3K27M, 102 days, H3.3WT, 101.5 days,  $p = .7796$ , log-rank test,) or Otv-a-Cre mice (Figure 2c, not reached median survival,  $p = .3677$ , log-rank test).

We observed tumors in the midbrain, pons, thalamus, hypothalamus, and the cerebellum in Otv-a-Cre mice injected with RCAS-PDGF-B and RCAS-H3.3K27M or RCAS-H3.3WT. (Table S4). H&E-stained brain sections revealed increased necrosis, microvascular proliferation, mitosis, and higher overall cell density both in H3.3K27M and H3.3WT tumors (Figure 2d). Most tumors showed WHO grade III or IV histology except for H3.3WT and p53WT tumors, where 58.3% (7/12) were WHO grade II (Figure 2e). We also found that 94.7% ( $n = 18/19$ ) of tumors in Otv-a-Cre;p53<sup>fl/fl</sup>; PDGF-B;H3.3K27M mice aggregated separately from the main tumor mass in the subependymal space of the lateral ventricle or the subcortical space, which was substantially higher than that in H3.3WT tumors (83.3%,  $n = 13/18$ ,  $p = .0897$ , Fisher's exact test). There was no difference in tumor dissemination between H3.3K27M and H3.3WT tumors in Otv-a-Cre;p53<sup>fl/+</sup>;PDGF-B (H3.3K27M, 63.6%, H3.3WT, 46.2%,  $p = .4442$ , Fisher's exact test) or Otv-a-Cre;p53<sup>+/+</sup>; PDGF-B mice (H3.3K27M, 42.9%, H3.3WT, 43.8%,  $p = 1.000$ , Fisher's exact test) (Figure 2f). Both H3.3K27M and H3.3WT tumors generated in Otv-a-Cre;p53<sup>fl/fl</sup> mice expressed the glioma markers Olig2 and Nestin in a majority of the cells as expected (Figure S2A,B), and GFAP to a lesser extent (Figure S2C). We also immunolabeled tumor tissue for the proliferative markers Ki67 and pH3Ser10 but there was no significant difference between H3.3K27M and H3.3WT tumors in all three p53 backgrounds (Figure 2g). IHC analysis revealed a significant decrease in H3K27me3 levels in H3.3K27M tumors compared with H3.3WT tumors in the Otv-a-Cre;p53<sup>fl/fl</sup> mice (% positive cells, H3.3K27M,  $5.5 \pm 2.6\%$ , H3.3WT,  $16.4 \pm 6.4\%$ ,  $p = .0196$ , Student's *t* test), but not in Otv-a-Cre;p53<sup>fl/+</sup> (H3.3K27M,  $7.8 \pm 6.8\%$ , H3.3WT,  $12.1 \pm 5.7\%$ ,  $p = .3767$ , Student's *t* test) or Otv-a-Cre;p53<sup>+/+</sup> (H3.3K27M,  $14.0 \pm 1.9\%$ , H3.3WT,  $13.7 \pm 4.1\%$ ,  $p = .9009$ , Student's *t* test) mice (Figure 2h). Thus, H3.3K27M overexpression in neonatal Olig2+ cells, when combined with PDGF-B overexpression and p53 loss, had minimal effects on tumor latency and cell proliferation, but decreased H3K27me3 levels and increased tumor grade relative to H3.3WT.

### 3.3 | H3.3K27M does not impact tumor latency or proliferation of PDGF-A-driven DIPG initiated in neonatal Olig2+ cells

PDGF-B overexpression has been widely used in mouse models of DIPG (Barton et al., 2013; Becher et al., 2010; Misuraca et al., 2016). However, recently published molecular meta-analysis shows that PDGF-B is rarely upregulated and/or amplified in human DIPG (Paugh et al., 2011; Puget et al., 2012), although PDGFRA alterations are frequently observed (Mackay et al., 2017). Therefore, we generated a GEMM of DIPG by overexpressing PDGF-A to selectively activate the PDGFRA signaling pathway (Westermarck et al., 1995). Otv-a-Cre;p53<sup>fl/fl</sup>;PDGF-A;H3.3K27M mice had significantly longer survival time compared with Otv-a-Cre;p53<sup>fl/fl</sup>; PDGF-B;H3.3K27M mice (Figure S3, median survival, PDGF-A, 56 days, PDGF-B, 31 days,  $p < .0001$ , log-rank test). Surprisingly, Otv-a-Cre;p53<sup>fl/fl</sup>;PDGF-A;H3.3K27M mice had a similar median survival as their H3.3WT counterparts (Figure 3a, median survival, H3.3K27M, 56 days, H3.3WT, 54 days,  $p = .7074$ , log-rank test). There was no correlation between survival and sex based on cox hazard regression analysis (Table S3). All the infected mice developed intracranial tumors, similar to the PDGF-B-based model, and the majority of the PDGF-A-driven tumors were observed in the brainstem (Table S5). All the H3.3K27M and H3.3WT tumors were classified as high-grade (Figure 3b,c). Similar to our observations in the PDGF-B-driven models, Olig2 and Nestin were expressed in a majority of the tumor cells, whereas GFAP showed only weak staining (Figure S2d-f). The fraction of Ki-67 positive cells in H3.3K27M tumors was slightly higher than in H3.3WT tumors, but the difference was not statistically significant (H3.3K27M,  $21.6 \pm 16.1\%$ , H3.3WT,  $14.9 \pm 12.5\%$ ,  $p = .2360$ , Student's *t* test) (Figure 3d). In addition, the fraction of pH3Ser10+ cells was similar between H3.3K27M and H3.3WT tumors (H3.3K27M,  $3.0 \pm 1.4\%$ , H3.3WT,  $3.1 \pm 1.0\%$ ,  $p = .9343$ , Student's *t* test) (Figure 3e). H3.3K27M tumors, however, had significantly lower H3K27me3-positivity than H3.3WT tumors (% H3K27me3+ cells, H3.3K27M,  $4.8 \pm 2.5\%$ , H3.3WT,  $9.2 \pm 3.7\%$ ,  $p = .0019$ , Student's *t* test) (Figure 3f). Thus, H3.3K27M does not affect tumor cell proliferation or tumor latency when tumors are induced with PDGF-A overexpression and p53 loss in Olig2+ cells, despite a significant loss of H3K27me3. These findings are similar to our PDGF-B driven model described above (Figure 2).

**FIGURE 2** H3.3K27M cooperates with PDGF-B to increase tumor malignancy and latency in Olig2+ cells. (a) Otv-a-Cre;p53<sup>fl/fl</sup>, (b) Otv-a-Cre;p53<sup>fl/+</sup>, and (c) Otv-a-Cre;p53<sup>+/+</sup> mice were injected with RCAS-PDGF-B and RCAS-H3.3K27M or RCAS-H3.3WT (PK, PDGF-B + H3.3K27M; PH, PDGF-B + H3.3 WT). Kaplan–Meier survival curves show a significant difference in median survival between Otv-a-Cre;p53<sup>fl/fl</sup>;PDGF-B;H3.3K27M and Otv-a-Cre;p53<sup>fl/fl</sup>;PDGF-B;H3.3WT mice.  $N = 21$  to 38, log-rank test. (d) Representative images of tumor tissue from the indicated mouse models, stained with H&E, or immunolabeled with antibodies against Ki67, pH3Ser10, and H3K27me3. Scale bar represents 50  $\mu\text{m}$ . (e) Tumor grading according to the diagnosis of diffuse astrocytoma based on WHO 2016 classification.  $N = 12$ , Fisher's exact test. (f) Tumor dissemination rates in the indicated mouse models.  $N = 13$  to 19, Fisher's exact test. (g, h). Quantification of percentages of Ki67+ (g) and H3K27me3+ (h) cells in H3.3K27M versus H3.3WT tumors in the three p53 backgrounds. Mean  $\pm$  SEM,  $n = 4$  to 5, Student's *t* test, ns, not significant

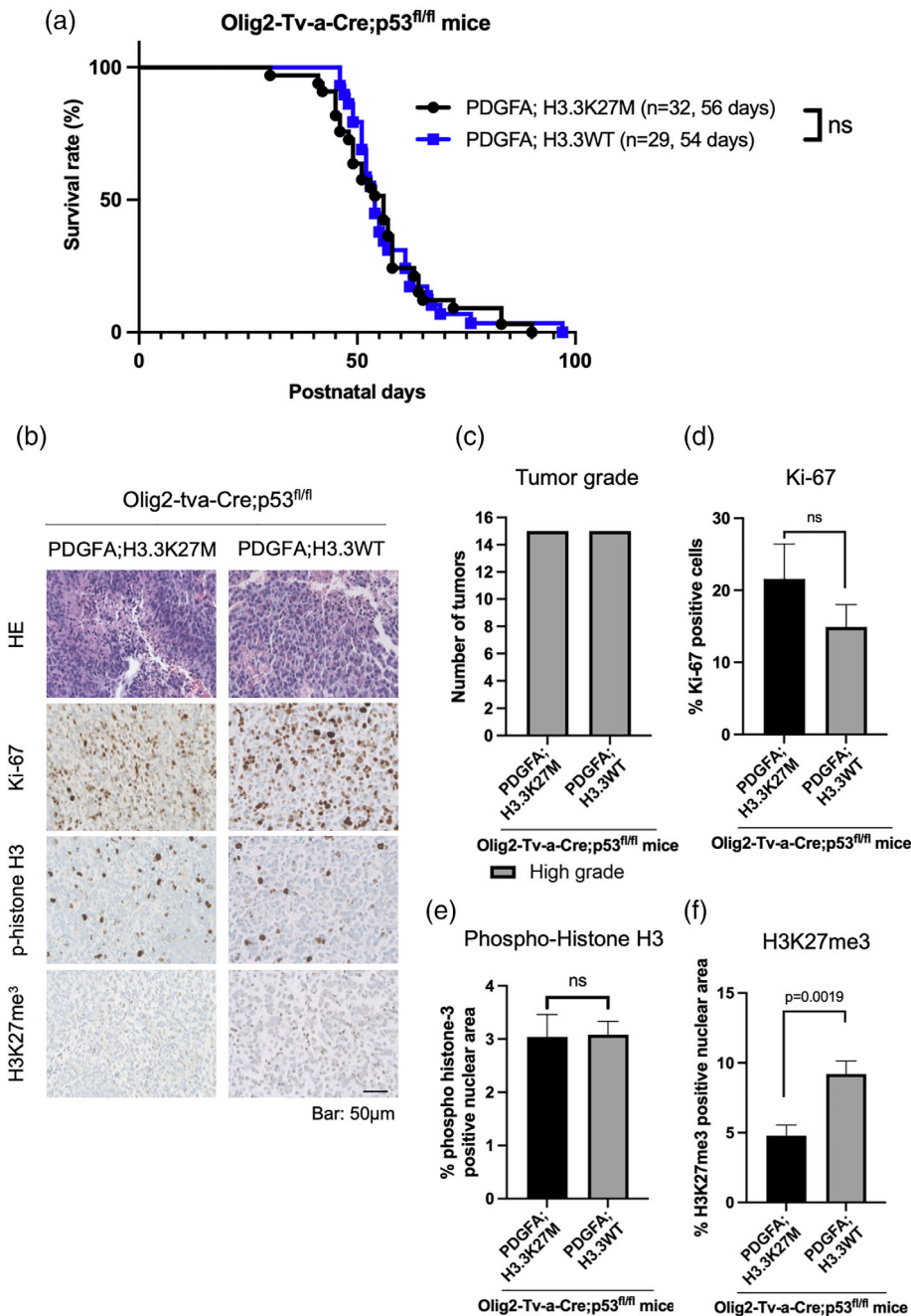


**FIGURE 3** H3.3K27M does not affect survival or tumor histology when co-expressed with PDGF-A in Olig2+ cells. (a) Kaplan–Meier survival curves of Otv-a-Cre;p53<sup>fl/fl</sup> mice injected with RCAS-PDGF-A and RCAS-H3.3K27M or RCAS-H3.3 WT.  $N = 29$  to 32, log-rank test. (b) Representative images of tumor tissue from the indicated mouse models, stained with H&E, or immunolabeled with antibodies against Ki67, pH3Ser10, and H3K27me3. (c) Tumor grading of the indicated tumors. H3.3K27M and H3.3WT tumors were both high-grade when induced with PDGF-A.  $N = 15$ , Fisher's exact test. (d–f) quantification of the percentages of Ki67+ (d), pH3Ser10 (e), and H3K27me3+ (f) cells in the indicated tumors. The percentage of H3K27me3+ cells was significantly reduced in H3.3K27M tumors relative to H3.3WT. Mean  $\pm$  SEM,  $n = 11$  to 16, Student's *t* test, ns, not significant

### 3.4 | H3.3K27M impacts tumor latency and proliferation of PDGF-A-driven DIPG initiated in neonatal nestin+ cells

Our results above show that H3.3K27M has little/no effects on tumor latency and proliferation both in PDGF-B- and PDGF-A-driven DIPG initiated in neonatal Olig2+ cells. But we have previously shown that H3.3K27M significantly decreases tumor latency and survival when tumors are initiated in Nestin+ progenitors (Cordero et al., 2017). These observations suggest that Nestin+ cells, rather than Olig2+ cells, are perhaps a more appropriate candidate cell-of-origin for H3K27M DIPG. As our previous study was done with PDGF-B

overexpression (Cordero et al., 2017), we generated a GEMM of DIPG based on PDGF-A overexpression to evaluate if H3.3K27M impacts mice survival and tumor histology in Nestin-Tv-a;p53<sup>fl/fl</sup> mice. Nestin-Tv-a;p53<sup>fl/fl</sup>;PDGF-A;H3.3K27M mice had significantly shorter survival than their H3.3WT counterparts (Figure 4a, median survival, H3.3K27M, 72.5 days, H3.3WT, 138 days,  $p = .0010$ , log-rank test). There was a significant correlation between H3.3K27M mutation and survival time based on cox hazard regression analysis (Table S3). The majority of the PDGF-A-driven tumors were observed in the brainstem, whereas one-third of Nestin-Tv-a;p53<sup>fl/fl</sup>;PDGF-A;H3.3WT mice did not form tumor at postnatal day 180 (Table S6). All the H3.3K27M and H3.3WT tumors were classified as high-grade



**FIGURE 4** H3.3K27M affects survival and tumor histology when co-expressed with PDGF-A in Nestin + cells. (a) Kaplan–Meier survival curves of Nestin-Tv-a;p53<sup>fl/fl</sup> mice injected with RCAS-PDGF-A, RCAS-Cre, and RCAS-H3.3K27M or RCAS-H3.3 WT. N = 24, log-rank test. (b) Representative images of tumor tissue from the indicated mouse models, stained with H&E, or immunolabeled with antibodies against Ki67, pH3Ser10, and H3K27me3. (c) Tumor grading of the indicated tumors. H3.3K27M and H3.3WT tumors were both high-grade when induced with PDGF-A. N = 8 to 11, Fisher's exact test. (d–f) Quantification of the percentages of Ki67+ (d), pH3Ser10+ (e), and H3K27me3+ (f) cells in the indicated tumors. The percentages of Ki67+, pH3Ser10+ were significantly increased and the percentage of H3K27me3+ cells were significantly reduced in H3.3K27M tumors relative to H3.3WT. Mean ± SEM, n = 8 to 11, Student's *t* test

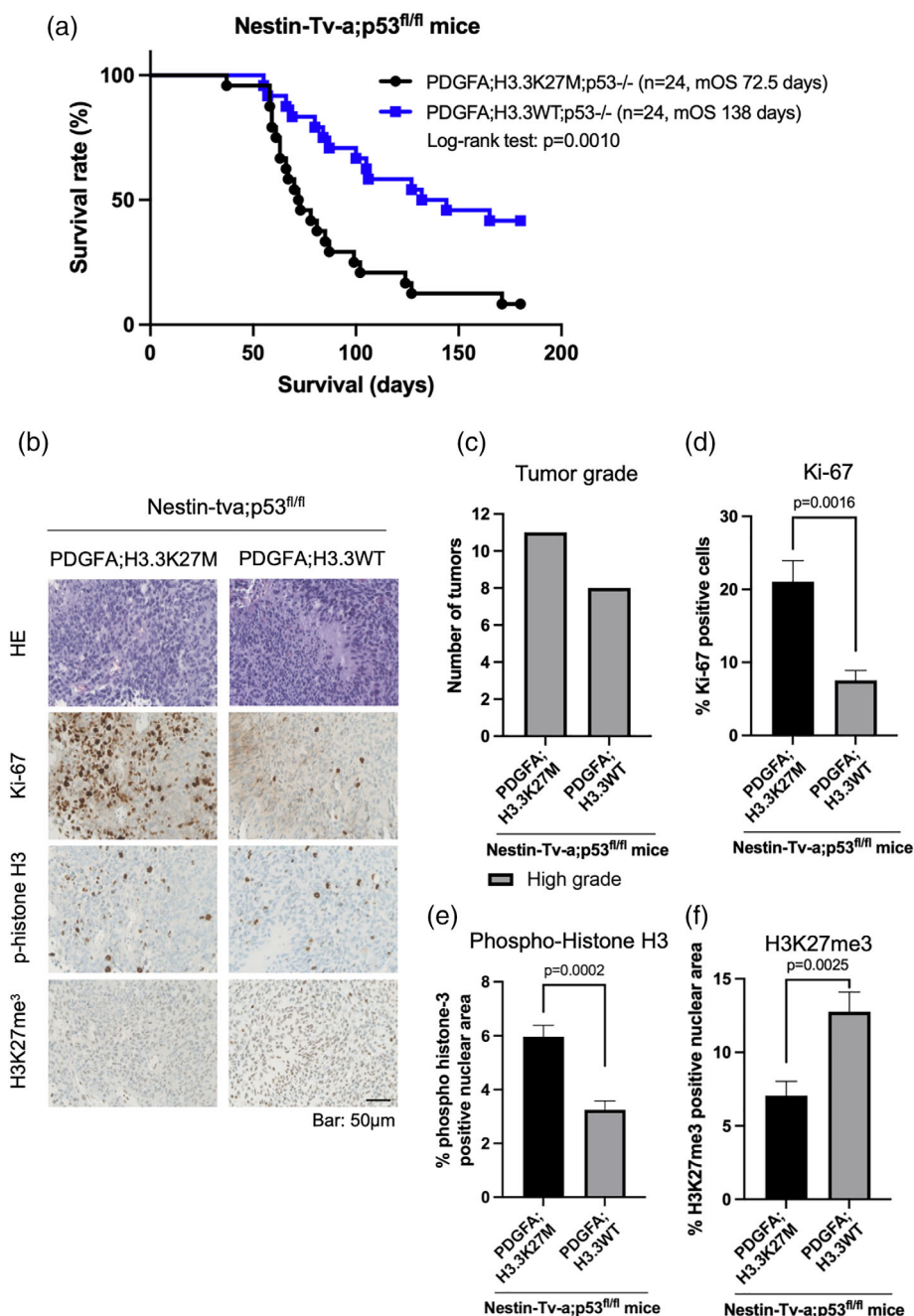


(Figure 4b,c). The fraction of Ki-67 positive cells in H3.3K27M tumors was significantly higher than in H3.3WT tumors (H3.3K27M, 21.1 ± 9.6%, H3.3WT, 7.5 ± 3.8%, *p* = .0016, Student's *t* test) (Figure 4d). Similar results were obtained with pH3Ser10 immunolabeling (H3.3K27M, 6.0 ± 1.4%, H3.3WT, 3.3 ± 0.9%, *p* = .0002, Student's *t* test) (Figure 4e). H3.3K27M tumors also had significantly lower H3K27me3-positivity than H3.3WT tumors (% H3K27me3+ cells, H3.3K27M, 7.1 ± 3.2%, H3.3WT, 12.8 ± 3.8%, *p* = .0025, Student's *t* test) (Figure 4f). Thus, H3.3K27M dramatically affects tumor cell proliferation and tumor latency when tumors are initiated in Nestin+ progenitors with p53 loss and PDGF-A overexpression as described above, or with p53 loss and PDGF-B overexpression (Cordero et al., 2017).

### 3.5 | Nestin-initiated tumors express higher levels of H3.3K27M than Olig2-initiated tumors

H3.3K27M, when combined with PDGF-A or PDGF-B, did not affect tumor aggressiveness when compared with H3.3WT in Otv-a-Cre; p53<sup>fl/fl</sup> mice, despite decreased H3K27me3 levels (Figures 2 and 3). In contrast, H3.3K27M significantly decreases tumor latency and survival when tumors are initiated in Nestin+ cells both in the PDGF-A-driven (Figures 4) and PDGF-B-driven models (Cordero et al., 2017). It is possible that there are only a few subsets of H3K27M+ cells in OPC-initiated tumors and, therefore, they do not drastically impact tumor latency and/or animal survival, or that H3K27M-positivity is not essential for tumorigenesis in the Otv-a-Cre mouse model. In

human H3.3K27M DIPG, the oncohistone is expressed in most tumor cells except for endothelial cells, vascular smooth muscle cells and lymphocytes (Bechet et al., 2014). Therefore, we evaluated H3.3K27M expression in tumors initiated in Otv-a-Cre;p53<sup>fl/fl</sup> mice and compared it with those from Ntv-a;p53<sup>fl/fl</sup> mice. Nestin-initiated tumors showed a higher fraction of H3K27M+ cells than Olig2-initiated tumors with PDGF-A overexpression (Ntv-a;p53<sup>fl/fl</sup>; PDGF-A, 91.0 ± 5.8%, Otv-a-Cre;p53<sup>fl/fl</sup>;PDGF-A, 45.6 ± 22.0%,  $p < .0001$ , ANOVA with Tukey's post hoc test) (Figure 5a,b). On the other hand, PDGF-B-derived tumors showed a smaller difference in H3K27M+ cells between the Ntv-a and Otv-a models, and this difference was not statistically significant (Ntv-a;p53<sup>fl/fl</sup>;PDGF-B, 38.3 ± 2.8%, Otv-a-Cre;p53<sup>fl/fl</sup>;PDGF-B, 16.9 ± 9.3%,  $p = .0885$ , ANOVA with Tukey's post hoc test). Also, we found increased H3K27M expression in PDGF-A tumors relative to PDGF-B tumors in both the Ntv-a; p53<sup>fl/fl</sup> (PDGF-A, 91.0 ± 5.8%, PDGF-B, 38.3 ± 2.8%,  $p = .0007$ , ANOVA with Tukey's post hoc test) and the Otv-a-Cre; p53<sup>fl/fl</sup> (PDGF-A, 45.6 ± 22.0%, PDGF-B, 16.9 ± 9.3%,  $p < .0001$ , ANOVA with Tukey's post hoc test) mice. Ross et al., 2020 have shown that PDGF-B-derived tumors have more tumor-associated monocytes than PDGF-A-derived tumors (Ross et al., 2020).

Therefore, we stained H3.3K27M-tumor tissues initiated in Otv-a-Cre;p53<sup>fl/fl</sup> mice with the microglial marker Iba1 to determine whether the difference in H3K27M positivity between PDGF-A and PDGF-B tumors is due to a difference in the microglial population (Hoeman et al., 2019; Ross et al., 2020), but found no significant difference between these two groups (PDGF-B, 10.5 ± 4.3%, PDGF-A, 7.9 ± 2.7%,  $p = .0835$ , Student's *t* test) (Figure S4A,B). Because exogenous H3K27M is tagged to GFP in our mouse models, we also stained tumor tissues with an antibody against GFP. The fraction of GFP+ cells was higher than that of H3K27M+ cells in all the tumor models except for Ntv-a;p53<sup>fl/fl</sup> mice with PDGF-A induction (Otv-a-Cre; p53<sup>fl/fl</sup>;PDGF-B; H3K27M, 16.9 ± 9.3%, GFP, 41.2 ± 13.7%; Otv-a-Cre;p53<sup>fl/fl</sup>;PDGF-A, H3K27M, 45.6 ± 22.0%, GFP 69.1 ± 19.8%; Ntv-a;p53<sup>fl/fl</sup>;PDGF-B, H3K27M, 38.3 ± 2.8%, GFP, 75.3 ± 8.6%; Ntv-a;p53<sup>fl/fl</sup>;PDGF-A, H3K27M, 91.0 ± 5.8%, GFP, 85.3 ± 5.0%) (Figure 5A), likely due to differential sensitivities of the two antibodies. Nonetheless, PDGF-B tumors in Otv-a-Cre;p53<sup>fl/fl</sup> mice had lower GFP expression than their counterparts in Ntv-a;p53<sup>fl/fl</sup> mice (Otv-a, 41.2 ± 13.7%, Ntv-a, 75.3 ± 8.6%,  $p = .0042$ , Student's *t* test) (Figure 5c). Otv-a-Cre;p53<sup>fl/fl</sup> PDGF-A tumors also had lower GFP staining than those in Ntv-a;p53<sup>fl/fl</sup> mice, although the difference was

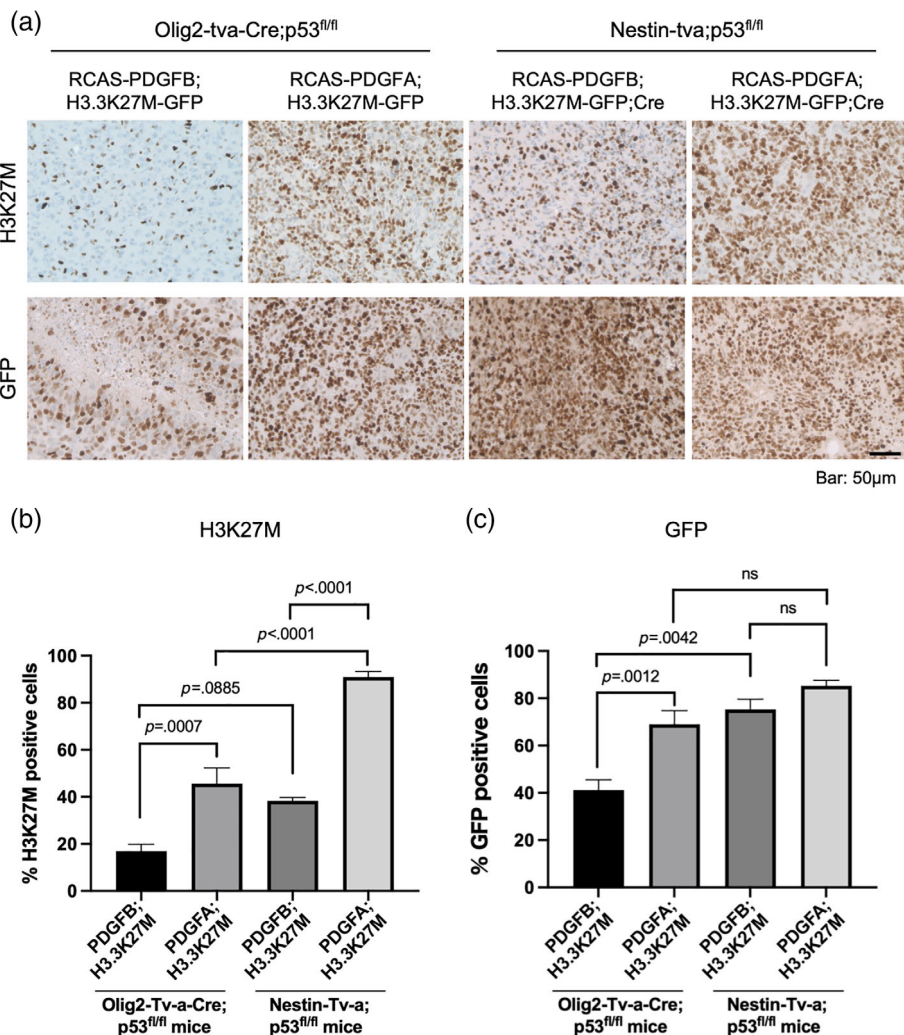
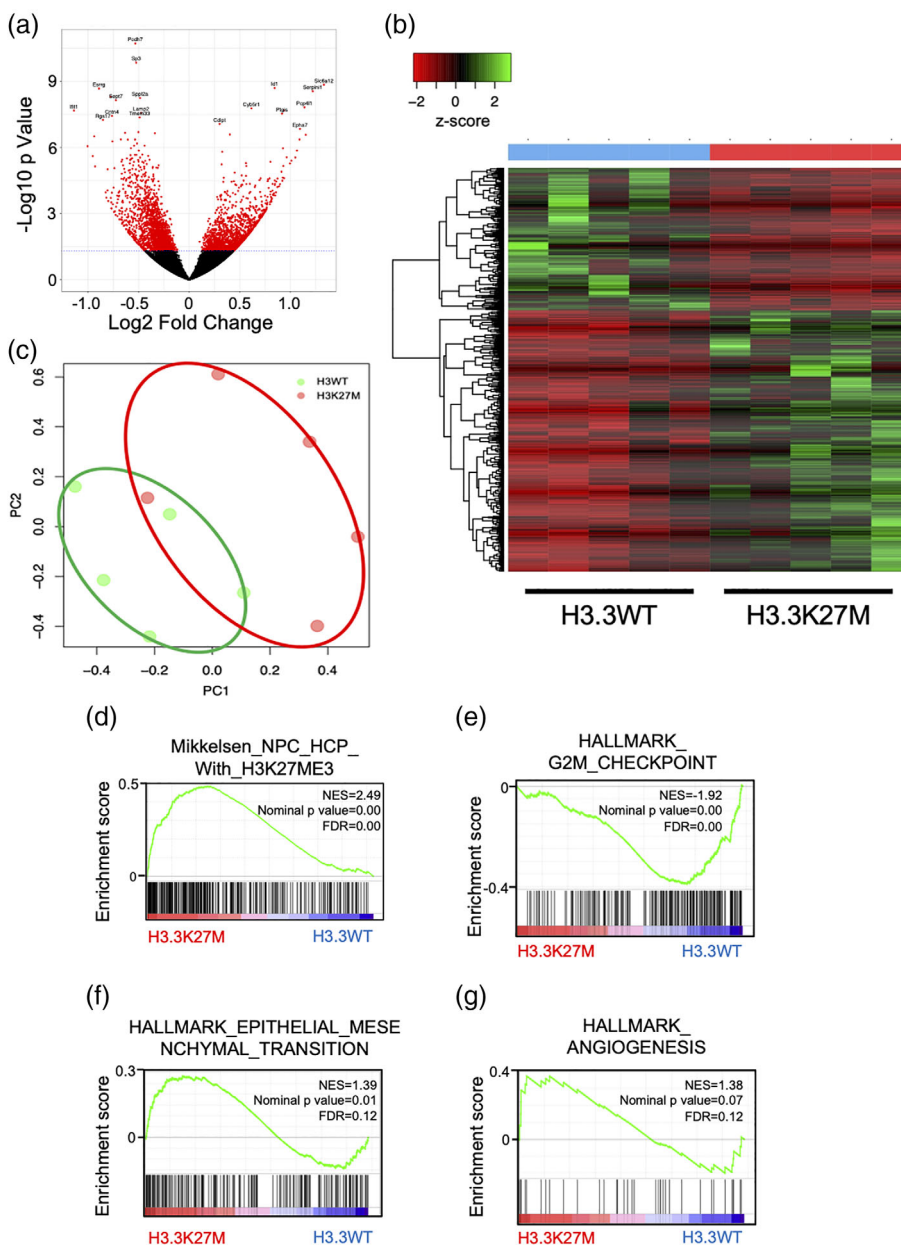


**FIGURE 5** Nestin and PDGF-A derived tumors express higher H3K27M levels than Olig2 and PDGF-B derived tumors. (a) Representative IHC images of tumor tissue from the indicated mouse models, stained with H3K27M and GFP antibodies. Otv-a-Cre;p53<sup>fl/fl</sup> mice were injected with RCAS-H3.3K27M-GFP and RCAS-PDGFB or RCAS-PDGFA. Ntv-a;p53<sup>fl/fl</sup> mice were injected with RCAS-H3.3K27M-GFP, Cre and RCAS-PDGFB or RCAS-PDGFA. (b, c). Quantification of the above IHC data showing percentages of H3K27M+ (b) and GFP+ (c) cells. PDGF-B-derived tumors in Ntv-a;p53<sup>fl/fl</sup> mice had higher levels of H3K27M+ and GFP+ cells than those in Otv-a-Cre;p53<sup>fl/fl</sup> mice. Similar differences can be seen between PDGF-A-derived tumors in Ntv-a;p53<sup>fl/fl</sup> mice relative to Otv-a-Cre;p53<sup>fl/fl</sup> mice. Mean ± SEM,  $n = 4$  to 12, ANOVA with Tukey's post hoc test, ns, not significant

**FIGURE 6** Transcriptomic analysis of Olig2-initiated tumors with PDGF-A overexpression. (a) Otv-a-Cre;p53<sup>fl/fl</sup> mice were injected with RCAS-PDGF-A and RCAS-H3.3K27M or RCAS-H3.3WT. Volcano plot comparing gene expression in H3.3K27M and H3.3WT tumors. There were a total of 907 significantly differentially expressed genes including 320 upregulated and 587 downregulated genes in the H3.3K27M group compared with the controls.  $N = 5$ . (b) Principal component analysis comparing Otv-a-Cre;p53<sup>fl/fl</sup>;PDGF-A;H3.3K27M and Otv-a-Cre;p53<sup>fl/fl</sup>;PDGF-A;H3.3WT tumors showing partial overlap. (c) Unsupervised hierarchical clustering of differentially regulated genes ( $p_{adj} < .05$ ) between H3.3K27M and H3.3WT tumors ( $n = 5$  each). (d) Gene ontology pathway analysis of upregulated and downregulated genes. (e–g) GSEA plots for interferon alpha response (e), interferon gamma response (f), and H3K27me3 promoters (g) (Mikkelsen et al., 2007) in H3.3K27M tumors relative to H3.3WT. NES, normalized enrichment score



not statistically significant (Otv-a,  $69.1 \pm 19.8\%$ , Ntv-a,  $85.3 \pm 5.0\%$ ,  $p = .2140$ , Student's  $t$  test). Thus, H3K27M is expressed at higher levels in PDGF-A relative to PDGF-B tumors, and when tumors are initiated in Nestin<sup>+</sup> cells relative to Olig2<sup>+</sup> cells.

### 3.6 | H3.3K27M has a significant effect on the transcriptome in PDGFA-driven gliomas initiated in Olig2<sup>+</sup> and Nestin<sup>+</sup> cells

To determine whether H3.3K27M impacts the tumor transcriptome, we performed RNA-seq analysis of PDGF-B-induced brainstem tumors in Otv-a-Cre;p53<sup>fl/fl</sup> mice expressing either H3.3WT or H3.3K27M (H3.3WT, two females and three males; H3.3K27M, three females and two males). Unsupervised hierarchical clustering and principal

component analysis showed that the majority of H3.3K27M tumors overlapped with H3.3WT tumors (Figure S5A,B), and there was not an apparent correlation between sex and the expression pattern (data not shown). Using a false discovery rate of  $\leq 0.05$ , we identified 25 significantly differentially expressed genes in H3.3K27M tumors, 23 of which were upregulated (Figure S5C, Table S7). We performed qRT-PCR analysis of all of these genes, but only Gm2694 and Egr4 were significantly downregulated (Figure S5D). Interestingly, GSEA analysis showed significant positive enrichment in oligodendrocyte markers and myelin sheath (Figure S5E,F, Table S8). Thus, H3.3K27M had a modest effect on the transcriptome of PDGF-B-induced DIPG relative to H3.3WT when initiated in Olig2<sup>+</sup> cells, although the heterogeneity in tumor locations might be a contributing factor (Table S4).

Next, we performed RNA-seq analysis of PDGF-A-induced tumors from Otv-a-Cre;p53<sup>fl/fl</sup> mice expressing H3.3WT or H3.3K27M



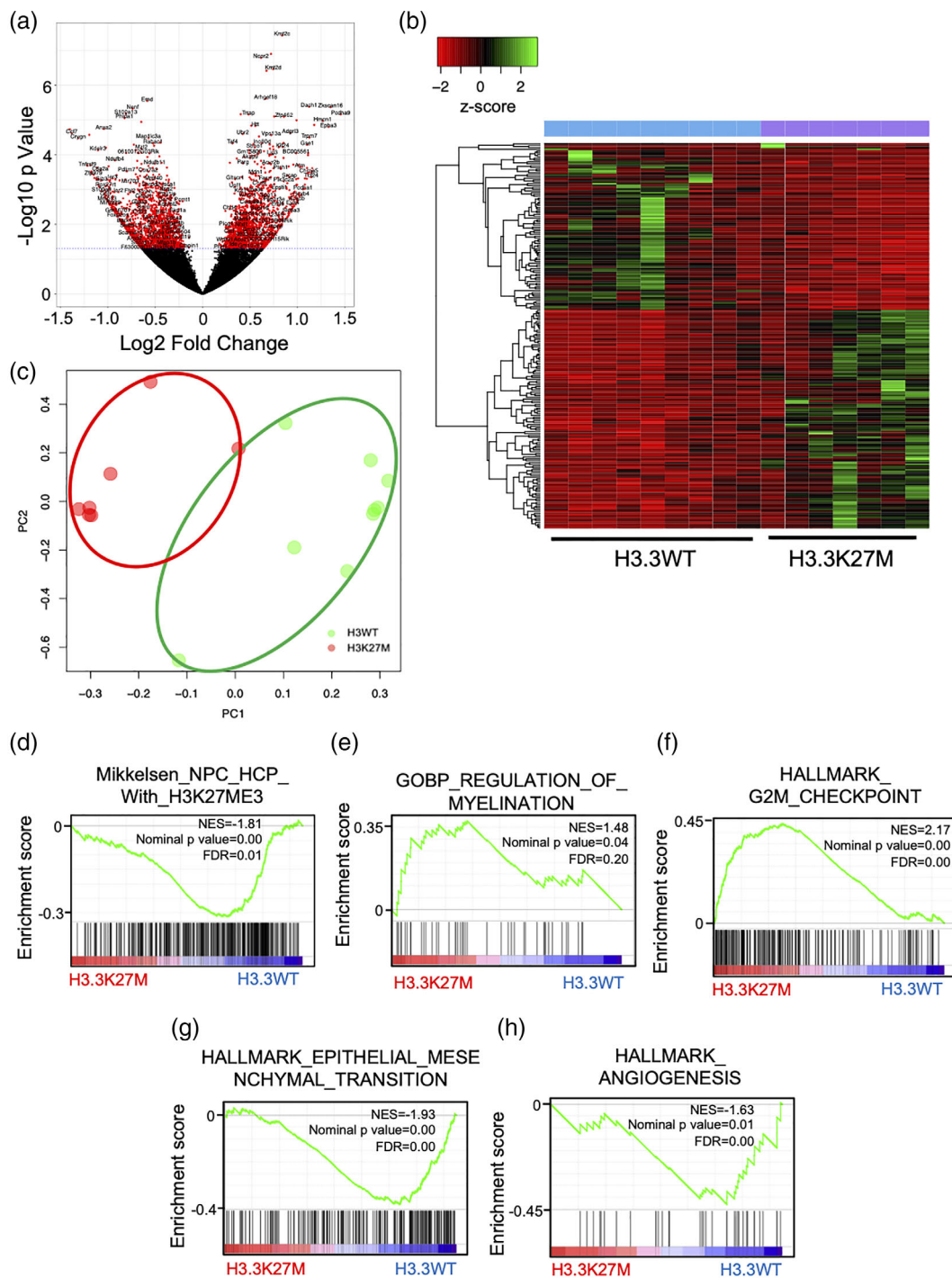


**FIGURE 7** Transcriptomic analysis of nestin-initiated tumors with PDGF-A overexpression. (a) *Ntv-a;p53<sup>fl/fl</sup>* mice were injected with RCAS-PDGF-A, RCAS-Cre, and RCAS-H3.3K27M or RCAS-H3.3WT. Volcano plot comparing gene expression of H3.3K27M and H3.3WT tumors. There were a total of 213 significantly differentially expressed genes including 123 upregulated and 90 downregulated genes in the H3.3K27M group compared with the controls.  $N = 7$  to 9. (b) Principal component analysis comparing *Ntv-a;p53<sup>fl/fl</sup>*;PDGF-A;H3.3K27M and *Ntv-a;p53<sup>fl/fl</sup>*;PDGF-A;H3.3WT tumors showing partial overlap. (c) Unsupervised hierarchical clustering of differentially regulated genes ( $p_{adj} < .05$ ) between H3.3K27M and H3.3WT tumors ( $n = 7$  to 9). (d-f) GSEA plots for inflammatory response (d), mitotic spindle (e), and H3K27me3 promoters (f) (Mikkelsen et al., 2007) in H3.3K27M tumors relative to H3.3WT. NES, normalized enrichment score

(H3.3WT, two females and three males; H3.3K27M, two females and three males). In contrast to the PDGF-B-based model, we found a total of 907 significantly differentially expressed genes including

320 upregulated and 587 downregulated genes in the H3.3K27M group compared with the controls, although fold changes in expression were small (Figure 6a, Table S9). Unsupervised hierarchical clustering



and principal component analysis showed that H3.3K27M tumors overlapped partially with H3.3WT tumors (Figure 6b,c). Gene ontology using DAVID software indicated that the upregulated genes were enriched in several processes including “cell adhesion” and “cell proliferation” (Figure S6). Using normalized expression data, we conducted GSEA analysis to further examine the effects of H3.3K27M on the transcriptome focusing on features of DMG cells including cell proliferation, epithelial-to-mesenchymal transition (EMT), and angiogenesis (Table S10). We identified a significant correlation between H3.3K27M and upregulation of genes characterized by H3K27 trimethylation and high-CpG-density promoters (Mikkelsen et al., 2007) (Figure 6d). As for the DMG features, H3.3K27M correlated with a significant downregulation of G2M checkpoint gene sets (Figure 6e), upregulation of EMT (Figure 6f), and upregulation of angiogenesis (Figure 6g). These results show that H3.3K27M promotes transcriptional changes consistent with known features of DMG in this model initiated in Olig2+ cells.

We compared the above RNA-seq data with transcriptomic analysis of tumors obtained by overexpressing PDGF-A, along with H3.3WT or H3.3K27M, in *Ntv-a;p53<sup>fl/fl</sup>* mice (H3.3WT, six females and three males; H3.3K27M, three females and three males). We found 213 significantly differentially expressed genes including 123 upregulated and 90 downregulated genes in the H3.3K27M group compared with the controls (Figure 7a, Table S11). Similar to PDGF-A tumors initiated in *Otv-a-Cre;p53<sup>fl/fl</sup>* mice, unsupervised hierarchical clustering and principal component analysis showed that H3.3K27M tumors overlapped partially with H3.3WT tumors (Figure 7b,c). Using GSEA analysis (Table S12), we identified a significant correlation between H3.3K27M and downregulation of genes characterized by H3K27 trimethylation and high-CpG-density promoters (Mikkelsen et al., 2007) (Figure 7d) and upregulation of genes related to oligodendrocyte differentiation and myelination (Figure 7e), which were opposite changes compared with PDGF-A-induced tumors from *Otv-a-Cre;p53<sup>fl/fl</sup>* mice (Figure 6d). As for the DMG features, interestingly, H3.3K27M was correlated to a significant upregulation of G2M checkpoint gene sets (Figure 7f), downregulation of EMT (Figure 7g), and downregulation of angiogenesis (Figure 7h). Similar to the tumors in *Otv-a-Cre;p53<sup>fl/fl</sup>* mice, we did detect a significant correlation between H3.3K27M and negative regulation of the *TNFA\_Signaling\_Via\_NFKB* gene set, and interestingly, only the H3.3K27M tumors initiated in Nestin+ cells but not Olig2+ cells were negatively enriched for the apoptosis gene set. These results suggest that the molecular effects of H3K27M in tumors initiated in Nestin+ and Olig2+ progenitors are distinct.

## 4 | DISCUSSION

Several studies have suggested that neonatal OPCs are a likely cell-of-origin for DIPG (Filbin et al., 2018; Monje et al., 2011). Single cell RNA-seq of human DIPG samples has shown that H3K27M DIPG tumors primarily contain OPC-like cells (Filbin et al., 2018). The basic helix-loop-helix transcription factor Olig2 is widely expressed in proliferating cells in the pons (Tate et al., 2015) and is highly expressed in

70%–80% of DIPG samples (Puget et al., 2012). Anderson et al. have shown that only DIPG cell lines retaining Olig2 could form robust Olig2-positive brainstem glioma (Anderson et al., 2017). We and others have previously published DIPG models arising from Nestin+ progenitors (Cordero et al., 2017; Larson et al., 2019), which also include OPCs and other progenitor cell populations (Walker et al., 2010). But there are no GEMMs characterizing midline gliomas initiated in OPCs. Here, we established GEMMs of DIPG initiated in Olig2+ cells.

We generated a murine DIPG model by overexpressing H3.3K27M and PDGF-B or PDGF-A, and by incorporating p53 loss into Olig2+ cells. Surprisingly, our data show that H3.3K27M has almost no effect on mice survival or cell proliferation relative to H3.3WT. In addition, we observed a significantly higher fraction of H3K27M+ cells in murine DIPG initiated in Nestin+ cells than those in Olig2+ cells, both in PDGF-A and PDGF-B models (Figure 5). Given that the H3.3K27M mutation is thought to initiate DIPG pathogenesis, our results are consistent with the observations by Haag et al. that NSCs are a more likely candidate for DIPG cell-of-origin for H3.3K27M mutant DIPG. Haag et al. investigated the biological effects of H3.3K27M in different human progenitor cell types of the neural lineage, and showed that NSCs but not OPCs give rise to tumors when induced with H3.3K27M and p53 inactivation in an orthotopic xenograft model (Haag et al., 2021). This is also in agreement with our previous work showing an oncogenic effect of H3.3K27M when combined with PDGF-B and p53 loss in Nestin+ progenitors (Cordero et al., 2017). Mackay et al. previously described the genomic profiles of 157 cases of pediatric high-grade glioma and showed that H3.3K27M coexisted with *PDGFRA* amplifications in many of the ventral pons tumors (Mackay et al., 2017). Also, Haag et al. showed that many OPC-like genes were upregulated in human NSCs with H3.3K27M induction (Haag et al., 2021). If the primary role of H3.3K27M is to differentiate NSCs into OPC-like cells and thereby initiate DIPG, both H3.3WT and H3.3K27M might have similar capacities for gliomagenesis in our DIPG models initiated in Olig2+ cells. In the context of previously reported single cell sequencing data of human DMG, while OPCs have been suggested as cells-of-origin, it is difficult to discern if the transcripts expressed in the human tumor cells expressing H3.3K27M reflect the cell-of-origin versus effects of genetic drivers such as H3.3K27M. Our study suggests that Nestin-expressing cells (NSCs) may also be candidate cells-of-origin in addition to OPCs, and that regardless of the cell-of-origin, most of the tumor cells end up adopting a transcriptome that is most similar to OPCs. Our data also suggests that in certain contexts, H3.3K27M can promote expression of transcripts consistent with an oligodendroglial cell fate. In the p53 WT model, H3.3K27M tumors were noted to be higher grade, but this did not translate into a significant survival benefit. Even in the human disease, tumor grade does not always correlate with survival (Buczkwicz et al., 2014). Also, H3.3K27M significantly altered the transcriptome and upregulated genes characterized by H3K27me3, relative to H3.3WT (Figure 6). This suggests that H3.3K27M impacts gene-expression in DIPG initiated in Olig2+ cells, but its effects on tumorigenesis are difficult to discern with relatively crude measurements such as histological and survival analyses.



The number of significant differentially expressed genes between H3.3K27M mutant tumors and H3.3WT control tumors was relatively small in our analysis relative to analysis in the human disease. Our data showed that H3.3K27M significantly changed the expression of 907 genes in *Otv-a-Cre;p53<sup>fl/fl</sup>* mice model, which was still much smaller than the number of significantly differentially expressed genes altered by H3.3K27M in human DIPG specimens. The plausible explanation is that human DIPG likely develop more slowly with sequential acquisition of genetic alterations while in the mouse modeling we are introducing three genetic alterations at the same time into the same cell-of-origin. The cell-of-origin and genetic alterations in the human disease besides H3.3K27M are likely heterogeneous across tumors while in the mouse modeling the co-genetic drivers are identical- PDGFA or PDGFB and p53 loss as well as the cell-of-origin. Looking at published data of human tumors where investigators compared H3.3K27M mutant human high-grade glioma to H3.3WT high-grade gliomas, we note some differences and some similarities between our observations in our genetic models and the reported effects of H3.3K27M in patient data. For example, a recent comparison of human H3.3K27M pediatric high-grade glioma to non-K27M pediatric high-grade gliomas identified the following top 5 Hallmark GSEA pathways to be significantly enriched in K27M tumors: myogenesis, UV response down, Kras signaling down, EMT, and estrogen response late (Sanders et al., 2020). Interestingly, three of these were significantly enriched in our analysis comparing H3.3K27M to H3.3WT tumors initiated in *Olig2*-expressing progenitors: (1) myogenesis (2) Kras signaling down, and (3) EMT while only one of these, UV response down was significantly enriched in our analysis comparing H3.3K27M to H3.3WT tumors initiated in *Nestin*-expressing progenitors. This highlights that the effects of H3.3K27M depends on the cell-of-origin and provides support for *Olig2* as a candidate marker for the cell-of-origin.

Surprisingly, RNA-seq comparison between *Otv-a-Cre;PDGF-A;p53<sup>fl/fl</sup>* and *Ntv-a; PDGF-A;p53<sup>fl/fl</sup>* tumors (Figures 6, 7, S7A,B, Table S13) demonstrated an absence of overlap between significantly differentially expressed genes in H3.3K27M versus H3.3WT tumors in the two models. The most likely explanation for this result is that the transcriptomal effects of H3.3K27M are context dependent and the chromatin state of *nestin*-expressing cells and *olig2*-expressing cells is quite different. Interestingly, gene sets promoting oligodendrocyte differentiation and/myelination were positively enriched in *Ntv-a;PDGF-A;p53<sup>fl/fl</sup>* tumors but were negatively enriched in *Otv-a-Cre;PDGF-A;p53<sup>fl/fl</sup>* tumors, suggesting that H3.3K27M could promote oligodendroglial cell fate when tumorigenesis is initiated in cells not already committed to become OPCs. Interestingly in the context of tumors initiated with PDGFA, the gene sets related to G2M checkpoint and mitotic spindle were significantly positively enriched by H3.3K27M in *Ntv-a* tumors while EMT, and angiogenesis were negatively enriched. By contrast, the G2M checkpoint and mitotic spindle gene sets were negatively enriched by H3.3K27M in the *Otv-a* tumors while EMT, and angiogenesis were positively enriched. There were also similarities between the two models. For example, inflammatory response and

*TNFA\_Signaling\_Via\_NFKB* gene sets were negatively enriched by H3.3K27M in both models. Interestingly, apoptosis gene set was negatively enriched in H3.3K27M tumors initiated in *Nestin*<sup>+</sup> cells but not *Olig2*<sup>+</sup> cells. We conclude that there are significant differences in the effects of H3.3K27M on tumor transcriptome between the *Ntv-a;p53<sup>fl/fl</sup>* and *Otv-a-Cre;p53<sup>fl/fl</sup>* models, despite some overlap between the two markers (Figure 1), suggesting that DIPG tumors in the *Otv-a-Cre;p53<sup>fl/fl</sup>* mice do not originate solely from *Nestin*<sup>+</sup>/*Olig2*<sup>+</sup> double-positive cells.

Interestingly, hypoxia pathway was significantly negatively enriched by H3.3K27M when tumorigenesis was initiated in *Nestin*-expressing progenitors but was neither significantly positively nor negatively enriched when tumorigenesis was initiated in *Olig2*-expressing progenitors. Angiogenesis, which is normally activated by hypoxia was significantly enriched in H3.3K27M tumors in *Otv-a-Cre;p53<sup>fl/fl</sup>* mice. *TNFA*-signaling, in contrast, was negatively enriched with H3.3K27M in both *Otv-a-Cre;p53<sup>fl/fl</sup>* mice and *Ntv-a;p53<sup>fl/fl</sup>* mice. This may be surprising as *TNFA*-signaling via *NFKB* has been associated with EMT in adult glioblastomas (Bhat et al., 2013), but as EMT is significantly positively enriched when tumorigenesis is initiated in *Olig2* positive cells but *TNFA*-signaling via *NFKB* is negatively enriched, it suggests that the mechanism for EMT is independent of *TNF-A* signaling via *NFKB* in the DMG model initiated in *Olig2*-expressing cells.

Tumors with PDGF-B overexpression and p53 loss dramatically shorten mouse survival compared with those with PDGF-B overexpression alone, regardless of H3.3 status in the *Otv-a-Cre;p53<sup>fl/fl</sup>* mice (Figure 2), consistent with our previous observations in the *Ntv-a;p53<sup>fl/fl</sup>* mice (Cordero et al., 2017). In addition, in mice overexpressing PDGF-B, our IHC data show a significantly lower level of H3K27me3 in H3.3K27M tumors relative to H3.3WT tumors with p53 deletion, but not with p53 intact (Figure 2). The above data suggest that H3.3K27M and p53 loss may cooperate to change the gene-expression profile of tumors originating in *Olig2*<sup>+</sup> cells. However, we could not generate tumors with H3.3K27M overexpression and p53 loss in the absence of PDGF-B overexpression, consistent with our previous study in neonatal brainstem *Nestin*<sup>+</sup> cells, where these two genetic alterations alone produced proliferating ectopic cell clusters but not gliomas (Cordero et al., 2017; Lewis et al., 2013). Future studies examining DIPG generation without PDGF signaling will help delineate the roles of p53 loss and H3.3K27M in gliomagenesis.

The median survival of *Otv-a-Cre;PDGF-B;p53<sup>fl/fl</sup>* mice was 31 days, which is significantly shorter than 51 days in *Otv-a-Cre;PDGF-A;p53<sup>fl/fl</sup>*. Also, IHC results showed that the fraction of H3K27M<sup>+</sup> cells was significantly lower in *Otv-a-Cre;PDGF-B;p53<sup>fl/fl</sup>* mice than *Otv-a-Cre;PDGF-A;p53<sup>fl/fl</sup>* (Figure 5). Moreover, bulk RNAseq showed that H3.3K27M significantly changed the expression of only 25 genes in *Otv-a-Cre;PDGF-B;p53<sup>fl/fl</sup>* tumors, which is much lower than 907 genes in *Otv-a-Cre;PDGF-A;p53<sup>fl/fl</sup>* tumors (Figures 6 and S5). It is possible that PDGF-B or other factors induced by PDGF-B overwhelm the effects of H3.3K27M in *Otv-a-Cre;PDGF-B;p53<sup>fl/fl</sup>* tumors. Previous reports have shown that

PDGF-B can bind to and activate both PDGFRA and PDGFRB, whereas PDGF-A binds to PDGFRA specifically (Nordby et al., 2017; Singh et al., 2002; Westermarck et al., 1995), suggesting that PDGF-B likely activates more robust downstream signaling relative to PDGF-A. Ross et al. recently reported potent inflammatory effects of PDGF-B in addition to poor survival in a cerebral cortex glioma model (Ross et al., 2020). The authors induced high-grade gliomas in Nestin+ cells by PDGF-A or PDGF-B overexpression with *Cdkn2a* or *Tp53* deletions and showed that PDGF-B increased tumor-associated macrophage recruitment via production of chemokines. However, our IHC data showed only a small, non-significant difference in the percentage of Iba1-positive cells, a well-known macrophage, and microglial marker, between PDGF-B- and PDGF-A-derived tumor tissues (Figure S4). Therefore, it is possible that the capacity of PDGF-B to recruit macrophages is spatiotemporal and dependent on the cell-of-origin.

The strength of our new Otv-a-Cre model is that PDGF overexpression and p53 loss resulted in diffuse gliomas in almost all the infected mice, supporting the idea that tumor cells with OPC-like features could have an important role in forming DIPG. In addition, our Otv-a-Cre model of DIPG displays similar latency and penetrance when compared with our previously reported Ntv-a model (Cordero et al., 2017). However, there are also several limitations to our study. First, we did not evaluate the interactions of Olig2+ tumor cells with other cell populations such as Nestin+ cells. Second, we have not investigated whether more differentiated cells that express Olig2, for example, mature oligodendrocytes, could serve as a cell-of-origin for DIPG, though we consider that possibility unlikely. As with any RCAS/Tv-a model, viral injections infect multiple cells, and it is likely that several different types of Olig2+ cells in the mouse brainstem are infected simultaneously with each injection. Third, there was significant variability in the tumor locations. This may be a technical issue as it is possible that a subset of the virus producing cells end up in the fourth ventricle with our hind-brain injections and can migrate throughout the ventricular system. This can reduce the number of significant differentially expressed genes. Finally, there are the potential limitations of our models in this research with respect to the requirement for PDGF signaling for tumorigenesis, and to the precursor populations that present in the brainstem at the time of injection expressing Olig2, Nestin, or both. PDGF-A/B signals are strong enough to generate tumors, which might make it difficult to evaluate the effect of H3.3K27M on the survival time in Otv-a-Cre;p53<sup>fl/fl</sup> mice. Despite these limitations, our novel DIPG mouse will have tremendous utility in preclinical drug studies given reproducible DIPG formation with PDGF overexpression and p53 loss.

In conclusion, we have described a novel GEMM of DIPG initiated in neonatal Olig2+ progenitors. As the majority of Olig2+ cells in the neonatal brainstem expressed *sox2* and were negative for *nestin* and as Lindquist et al. demonstrated that the majority of Olig2 + *Sox2*+ pontine cells also express OPC markers such as PDGFRA and *Sox10* (Lindquist et al., 2016), these cells are therefore most consistent with

OPCs. There was no significant effect of H3.3K27M on tumor latency or proliferation despite reduced H3K27me3 levels in the mutant tumors relative to H3.3WT, which contrasts with our observations with tumors initiated in Nestin+ progenitors. H3.3K27M significantly altered similar cellular pathways in tumors initiated in Olig2+ and Nestin+ cells, most notably in inhibition of inflammation and interferon signaling suggesting that one of the key roles of H3.3K27M may be immunosuppression. However, there was little/no overlap in significantly differentially expressed genes between these two models. Our results strongly suggest that the oncogenic and transcriptomic effects of H3.3K27M are dependent on the tumor cell-of-origin. Future studies investigating epigenetic changes induced by H3.3K27M in different cells-of-origin will improve our understanding of DIPG pathogenesis.

#### AUTHOR CONTRIBUTIONS

Yusuke Tomita: Writing draft, creating figures/tables, Survival analysis and RNA-seq of PDGFA-derived tumors with Olig2-Tv-a-Cre; p53<sup>fl/fl</sup> mice, immunostaining, IHC for all the samples, all the statistical analysis. Yosuke Shimazu: Survival analysis and RNA-seq of PDGF-B-derived tumors. Agila Somasundaram: Writing and editing draft. Yusuke Tomita: Cox regression analysis. Nozomu Takata: Immunostaining. Angelo Angione, Gonzalo Pinero, and Dolores Hambardzumyan: Triple Immunofluorescence and quantification for Nestin, Olig2 and Sox2. Yukitomo Ishi: Survival analysis of PDGF-A-derived tumors in Ntv-a;p53<sup>fl/fl</sup> mice, Daniel J. Brat: Histological analysis. Rintaro Hashizume: Survival analysis of PDGF-A-derived tumors in Ntv-a;p53<sup>fl/fl</sup> mice, Christine M. Hoeman: Survival analysis of PDGF-A-derived tumors in Ntv-a;p53<sup>fl/fl</sup> mice, optimization of GFP/Iba1-IHC, and qRT-PCR. Oren J. Becher: Conceived of this project and supervised the work.

#### ACKNOWLEDGMENTS

This work was supported by NIH grants K02 NS086917, R01 CA197313, R21 1R21NS114431-01, Rory David Deutsch Foundation, Madox's Warriors, DIPG Collaborative, the Cure Starts Now Foundation, the ChadTough Foundation, Cure Starts Now Australia, The Julian Boivin Courage for Cures Foundation, Hope for Caroline Foundation, Lauren's Fight for Cure Foundation, Aidan's Avengers Foundation, Austin Strong Foundation, Brooke Healey Foundation, Cure Brain Cancer Foundation, Grant's Ginormous Gift Foundation, Michael Mosier Defeat DIPG Foundation, Musella Foundation, Operation Grace White Foundation, Smiles for Sophie Foundation, Jeffrey Thomas Hayden Foundation, Pray Hope Believe Foundation, Ellie DIPG Research Fund, Julia Barbara Foundation, Ryan's Hope Foundation, Benny's World Foundation, Canadian Children's Brain Cancer Foundation, Reflections Of Grace Foundation, American Childhood Cancer Organization, Danni Kemp Cancer Research Fund, Love, Chloe Foundation, Smile for Brooklyn Foundation, The Kira Foundation, and the Wayland Villars DIPG Foundation.

#### CONFLICT OF INTEREST

The authors declare no competing financial interests.



## DATA AVAILABILITY STATEMENT

The data that support the findings of this study are available from the corresponding author upon reasonable request.

## ORCID

Yusuke Tomita <https://orcid.org/0000-0002-3964-823X>

Yosuke Shimazu <https://orcid.org/0000-0002-7696-7811>

Oren J. Becher <https://orcid.org/0000-0003-4016-8492>

## REFERENCES

- Anderson, J. L., Muraleedharan, R., Oatman, N., Klotter, A., Sengupta, S., Waclaw, R. R., Wu, J., Drissi, R., Miles, L., Raabe, E. H., Weirauch, M. L., Fouladi, M., Chow, L. M., Hoffman, L., DeWire, M., & Dasgupta, B. (2017). The transcription factor Olig2 is important for the biology of diffuse intrinsic pontine gliomas. *Neuro-Oncology*, 19(8), 1068–1078. <https://doi.org/10.1093/neuonc/now299>
- Barton, K. L., Misuraca, K., Cordero, F., Dobrikova, E., Min, H. D., Gromeier, M., Kirsch, D. G., & Becher, O. J. (2013). PD-0332991, a CDK4/6 inhibitor, significantly prolongs survival in a genetically engineered mouse model of brainstem glioma. *PLoS One*, 8(10), e77639. <https://doi.org/10.1371/journal.pone.0077639>
- Becher, O. J., Hambardzumyan, D., Walker, T. R., Helmy, K., Nazarian, J., Albrecht, S., Hiner, R. L., Gall, S., Huse, J. T., Jabado, N., MacDonald, T. J., & Holland, E. C. (2010). Preclinical evaluation of radiation and perifosine in a genetically and histologically accurate model of brainstem glioma. *Cancer Research*, 70(6), 2548–2557. <https://doi.org/10.1158/0008-5472.CAN-09-2503>
- Bechet, D., Gielen, G. G., Korshunov, A., Pfister, S. M., Rousso, C., Faury, D., Fiset, P. O., Benlimane, N., Lewis, P. W., Lu, C., David Allis, C., Kieran, M. W., Ligon, K. L., Pietsch, T., Ellezari, B., Albrecht, S., & Jabado, N. (2014). Specific detection of methionine 27 mutation in histone 3 variants (H3K27M) in fixed tissue from high-grade astrocytomas. *Acta Neuropathologica*, 128(5), 733–741. <https://doi.org/10.1007/s00401-014-1337-4>
- Bender, S., Tang, Y., Lindroth, A. M., Hovestadt, V., Jones, D. T., Kool, M., Zapatka, M., Northcott, P. A., Sturm, D., Wang, W., Radlwimmer, B., Højfeldt, J. W., Truffaux, N., Castel, D., Schubert, S., Ryzhova, M., Şeker-Cin, H., Gronych, J., Johann, P. D., ... Pfister, S. M. (2013). Reduced H3K27me3 and DNA hypomethylation are major drivers of gene expression in K27M mutant pediatric high-grade gliomas. *Cancer Cell*, 24(5), 660–672. <https://doi.org/10.1016/j.ccr.2013.10.006>
- Bhat, K. P. L., Balasubramanian, V., Vaillant, B., Ezhilarsan, R., Hummelink, K., Hollingsworth, F., Wani, K., Heathcock, L., James, J. D., Goodman, L. D., Conroy, S., Long, L., Lelic, N., Wang, S., Gumin, J., Raj, D., Kodama, Y., Raghunathan, A., Olar, A., ... Aldape, K. (2013). Mesenchymal differentiation mediated by NF- $\kappa$ B promotes radiation resistance in glioblastoma. *Cancer Cell*, 24(3), 331–346. <https://doi.org/10.1016/j.ccr.2013.08.001>
- Brien, G. L., Bressan, R. B., Monger, C., Gannon, D., Lagan, E., Doherty, A. M., Healy, E., Neikes, H., Fitzpatrick, D. J., Deevy, O., Grant, V., Marqués-Torrejón, M. A., Alfazema, N., Pollard, S. M., & Bracken, A. P. (2021). Simultaneous disruption of PRC2 and enhancer function underlies histone H3.3-K27M oncogenic activity in human hindbrain neural stem cells. *Nature Genetics*, 53(8), 1221–1232. <https://doi.org/10.1038/s41588-021-00897-w>
- Buczkwicz, P., & Hawkins, C. (2015). Pathology, molecular genetics, and epigenetics of diffuse intrinsic pontine glioma. *Frontiers in Oncology*, 5, 147. <https://doi.org/10.3389/fonc.2015.00147>
- Buczkwicz, P., Hoeman, C., Rakopoulos, P., Pajovic, S., Letourneau, L., Dzamba, M., Morrison, A., Lewis, P., Bouffet, E., Bartels, U., Zuccaro, J., Agnihotri, S., Ryall, S., Barszczyk, M., Chornenkyy, Y., Bourgey, M., Bourque, G., Montpetit, A., Cordero, F., ... Hawkins, C. (2014). Genomic analysis of diffuse intrinsic pontine gliomas identifies three molecular subgroups and recurrent activating ACVR1 mutations. *Nature Genetics*, 46(5), 451–456. <https://doi.org/10.1038/ng.2936>
- Chan, K. M., Fang, D., Gan, H., Hashizume, R., Yu, C., Schroeder, M., Gupta, N., Mueller, S., James, C. D., Jenkins, R., Sarkaria, J., & Zhang, Z. (2013). The histone H3.3K27M mutation in pediatric glioma reprograms H3K27 methylation and gene expression. *Genes & Development*, 27(9), 985–990. <https://doi.org/10.1101/gad.217778.113>
- Cordero, F. J., Huang, Z., Grenier, C., He, X., Hu, G., McLendon, R. E., Murphy, S. K., Hashizume, R., & Becher, O. J. (2017). Histone H3.3K27M represses p16 to accelerate Gliomagenesis in a murine model of DIPG. *Molecular Cancer Research*, 15(9), 1243–1254. <https://doi.org/10.1158/1541-7786.MCR-16-0389>
- Encinas, J. M., Vaahtokari, A., & Enikolopov, G. (2006). Fluoxetine targets early progenitor cells in the adult brain. *Proceedings of the National Academy of Sciences of the United States of America*, 103(21), 8233–8238. <https://doi.org/10.1073/pnas.0601992103>
- Filbin, M. G., Tirosh, I., Hovestadt, V., Shaw, M. L., Escalante, L. E., Mathewson, N. D., Neftel, C., Frank, N., Pelton, K., Hebert, C. M., Haberler, C., Yizhak, K., Gojo, J., Egervari, K., Mount, C., van Galen, P., Bonal, D. M., Nguyen, Q. D., Beck, A., ... Suvà, M. L. (2018). Developmental and oncogenic programs in H3K27M gliomas dissected by single-cell RNA-seq. *Science*, 360(6386), 331–335. <https://doi.org/10.1126/science.aao4750>
- Funato, K., Major, T., Lewis, P. W., Allis, C. D., & Tabar, V. (2014). Use of human embryonic stem cells to model pediatric gliomas with H3.3K27M histone mutation. *Science*, 346(6216), 1529–1533. <https://doi.org/10.1126/science.1253799>
- Haag, D., Mack, N., Benites Goncalves da Silva, P., Statz, B., Clark, J., Tanabe, K., Sharma, T., Jäger, N., Jones, D. T. W., Kawachi, D., Wernig, M., & Pfister, S. M. (2021). H3.3-K27M drives neural stem cell-specific gliomagenesis in a human iPSC-derived model. *Cancer Cell*, 39, 407–422.e13. <https://doi.org/10.1016/j.ccell.2021.01.005>
- Hargrave, D., Bartels, U., & Bouffet, E. (2006). Diffuse brainstem glioma in children: Critical review of clinical trials. *The Lancet Oncology*, 7(3), 241–248. [https://doi.org/10.1016/s1470-2045\(06\)70615-5](https://doi.org/10.1016/s1470-2045(06)70615-5)
- Hoeman, C. M., Cordero, F. J., Hu, G., Misuraca, K., Romero, M. M., Cardona, H. J., Nazarian, J., Hashizume, R., McLendon, R., Yu, P., Procissi, D., Gadd, S., & Becher, O. J. (2019). ACVR1 R206H cooperates with H3.1K27M in promoting diffuse intrinsic pontine glioma pathogenesis. *Nature Communications*, 10(1), 1023. <https://doi.org/10.1038/s41467-019-08823-9>
- Khuong-Quang, D. A., Buczkowicz, P., Rakopoulos, P., Liu, X. Y., Fontebasso, A. M., Bouffet, E., Bartels, U., Albrecht, S., Schwartzentruber, J., Letourneau, L., Bourgey, M., Bourque, G., Montpetit, A., Bourret, G., Lepage, P., Fleming, A., Lichter, P., Kool, M., von Deimling, A., ... Hawkins, C. (2012). K27M mutation in histone H3.3 defines clinically and biologically distinct subgroups of pediatric diffuse intrinsic pontine gliomas. *Acta Neuropathologica*, 124(3), 439–447. <https://doi.org/10.1007/s00401-012-0998-0>
- Larson, J. D., Kasper, L. H., Paugh, B. S., Jin, H., Wu, G., Kwon, C. H., Fan, Y., Shaw, T. I., Silveira, A. B., Qu, C., Xu, R., Zhu, X., Zhang, J., Russell, H. R., Peters, J. L., Finkelstein, D., Xu, B., Lin, T., Tinkle, C. L., ... Baker, S. J. (2019). Histone H3.3 K27M accelerates spontaneous brainstem glioma and drives restricted changes in bivalent gene expression. *Cancer Cell*, 35(1), 140–155.e7. <https://doi.org/10.1016/j.ccell.2018.11.015>
- Lewis, P. W., Müller, M. M., Koletsky, M. S., Cordero, F., Lin, S., Banaszynski, L. A., Garcia, B. A., Muir, T. W., Becher, O. J., & Allis, C. D. (2013). Inhibition of PRC2 activity by a gain-of-function H3 mutation found in pediatric glioblastoma. *Science*, 340(6134), 857–861. <https://doi.org/10.1126/science.1232245>



- Lindquist, R. A., Guinto, C. D., Rodas-Rodriguez, J. L., Fuentealba, L. C., Tate, M. C., Rowitch, D. H., & Alvarez-Buylla, A. (2016). Identification of proliferative progenitors associated with prominent postnatal growth of the pons. *Nature Communications*, 7, 11628. <https://doi.org/10.1038/ncomms11628>
- Louis, D. N., Perry, A., Reifenberger, G., von Deimling, A., Figarella-Branger, D., Cavenee, W. K., Ohgaki, H., Wiestler, O. D., Kleihues, P., & Ellison, D. W. (2016). The 2016 World Health Organization classification of tumors of the central nervous system: A summary. *Acta Neuropathologica*, 131(6), 803–820. <https://doi.org/10.1007/s00401-016-1545-1>
- Mackay, A., Burford, A., Carvalho, D., Izquierdo, E., Fazal-Salom, J., Taylor, K. R., Bjerke, L., Clarke, M., Vinci, M., Nandhabalan, M., Temelso, S., Popov, S., Molinari, V., Raman, P., Waanders, A. J., Han, H. J., Gupta, S., Marshall, L., Zacharoulis, S., ... Jones, C. (2017). Integrated molecular meta-analysis of 1,000 pediatric high-grade and diffuse intrinsic pontine glioma. *Cancer Cell*, 32(4), 520–537.e5. <https://doi.org/10.1016/j.ccell.2017.08.017>
- Mehta, S., Huillard, E., Kesari, S., Maire, C. L., Golebiowski, D., Harrington, E. P., Alberta, J. A., Kane, M. F., Theisen, M., Ligon, K. L., Rowitch, D. H., & Stiles, C. D. (2011). The central nervous system-restricted transcription factor Olig2 opposes p53 responses to genotoxic damage in neural progenitors and malignant glioma. *Cancer Cell*, 19(3), 359–371. <https://doi.org/10.1016/j.ccr.2011.01.035>
- Mikkelsen, T. S., Ku, M., Jaffe, D. B., Issac, B., Lieberman, E., Giannoukos, G., Alvarez, P., Brockman, W., Kim, T. K., Koche, R. P., Lee, W., Mendenhall, E., O'Donovan, A., Presser, A., Russ, C., Xie, X., Meissner, A., Wernig, M., Jaenisch, R., ... Bernstein, B. E. (2007). Genome-wide maps of chromatin state in pluripotent and lineage-committed cells. *Nature*, 448(7153), 553–560. <https://doi.org/10.1038/nature06008>
- Misuraca, K. L., Barton, K. L., Chung, A., Diaz, A. K., Conway, S. J., Corcoran, D. L., Baker, S. J., & Becher, O. J. (2014). Pax3 expression enhances PDGF-B-induced brainstem gliomagenesis and characterizes a subset of brainstem glioma. *Acta Neuropathologica Communications*, 2, 134. <https://doi.org/10.1186/s40478-014-0134-6>
- Misuraca, K. L., Hu, G., Barton, K. L., Chung, A., & Becher, O. J. (2016). A novel mouse model of diffuse intrinsic pontine glioma initiated in Pax3-expressing cells. *Neoplasia*, 18(1), 60–70. <https://doi.org/10.1016/j.neo.2015.12.002>
- Mohammad, F., Weissmann, S., Leblanc, B., Pandey, D. P., Højfeldt, J. W., Comet, I., Zheng, C., Johansen, J. V., Rapin, N., Porse, B. T., Tvardovskiy, A., Jensen, O. N., Olaciregui, N. G., Lavarino, C., Suñol, M., de Torres, C., Mora, J., Carcaboso, A. M., & Helin, K. (2017). EZH2 is a potential therapeutic target for H3K27M-mutant pediatric gliomas. *Nature Medicine*, 23(4), 483–492. <https://doi.org/10.1038/nm.4293>
- Monje, M., Mitra, S. S., Freret, M. E., Raveh, T. B., Kim, J., Masek, M., Attema, J. L., Li, G., Haddix, T., Edwards, M. S. B., Fisher, P. G., Weissman, I. L., Rowitch, D. H., Vogel, H., Wong, A. J., & Beachy, P. A. (2011). Hedgehog-responsive candidate cell of origin for diffuse intrinsic pontine glioma. *Proceedings of the National Academy of Sciences of the United States of America*, 108(11), 4453–4458. <https://doi.org/10.1073/pnas.1101657108>
- Nagaraja, S., Vitanza, N. A., Woo, P. J., Taylor, K. R., Liu, F., Zhang, L., Li, M., Meng, W., Ponnuswami, A., Sun, W., Ma, J., Hulleman, E., Swigut, T., Wysocka, J., Tang, Y., & Monje, M. (2017). Transcriptional dependencies in diffuse intrinsic pontine glioma. *Cancer Cell*, 31(5), 635–652.e6. <https://doi.org/10.1016/j.ccell.2017.03.011>
- Nordby, Y., Richardsen, E., Rakaee, M., Ness, N., Donnem, T., Patel, H. R., Busund, L. T., Bremnes, R. M., & Andersen, S. (2017). High expression of PDGFR- $\beta$  in prostate cancer stroma is independently associated with clinical and biochemical prostate cancer recurrence. *Scientific Reports*, 7, 43378. <https://doi.org/10.1038/srep43378>
- Paugh, B. S., Broniscer, A., Qu, C., Miller, C. P., Zhang, J., Tatevossian, R. G., Olson, J. M., Geyer, J. R., Chi, S. N., da Silva, N. S., Onar-Thomas, A., Baker, J. N., Gajjar, A., Ellison, D. W., & Baker, S. J. (2011). Genome-wide analyses identify recurrent amplifications of receptor tyrosine kinases and cell-cycle regulatory genes in diffuse intrinsic pontine glioma. *Journal of Clinical Oncology*, 29(30), 3999–4006. <https://doi.org/10.1200/jco.2011.35.5677>
- Puget, S., Philippe, C., Bax, D. A., Job, B., Varlet, P., Junier, M. P., Andreiulo, F., Carvalho, D., Reis, R., Guerrini-Rousseau, L., Roujeau, T., Dessen, P., Richon, C., Lazar, V., le Teuff, G., Sainte-Rose, C., Georger, B., Vassal, G., Jones, C., & Grill, J. (2012). Mesenchymal transition and PDGFRA amplification/mutation are key distinct oncogenic events in pediatric diffuse intrinsic pontine gliomas. *PLoS One*, 7(2), e30313. <https://doi.org/10.1371/journal.pone.0030313>
- Ross, J. L., Chen, Z., Herting, C. J., Grabovska, Y., Szulzewsky, F., Puigdelloses, M., Monterroza, L., Switchenko, J., Wadhvani, N. R., Cimino, P. J., Mackay, A., Jones, C., Read, R. D., MacDonald, T. J., Schniederjan, M., Becher, O. J., & Hambarzumyan, D. (2021). Platelet-derived growth factor beta is a potent inflammatory driver in paediatric high-grade glioma. *Brain*, 144, 53–69. <https://doi.org/10.1093/brain/awaa382>
- Sanders, L. M., Cheney, A., Seninge, L., van den Bout, A., Chen, M., Beale, H. C., Kephart, E. T., Pfeil, J., Learned, K., Lyle, A. G., Bjork, I., Haussler, D., Salama, S. R., & Vaske, O. M. (2020). Identification of a differentiation stall in epithelial mesenchymal transition in histone H3-mutant diffuse midline glioma. *Gigascience*, 9(12), 1–14. <https://doi.org/10.1093/gigascience/giaa136>
- Schüller, U., Heine, V. M., Mao, J., Kho, A. T., Dillon, A. K., Han, Y. G., Huillard, E., Sun, T., Ligon, A. H., Qian, Y., Ma, Q., Alvarez-Buylla, A., McMahon, A. P., Rowitch, D. H., & Ligon, K. L. (2008). Acquisition of granule neuron precursor identity is a critical determinant of progenitor cell competence to form Shh-induced medulloblastoma. *Cancer Cell*, 14(2), 123–134. <https://doi.org/10.1016/j.ccr.2008.07.005>
- Schwartzentruber, J., Korshunov, A., Liu, X. Y., Jones, D. T., Pfaff, E., Jacob, K., Sturm, D., Fontebasso, A. M., Quang, D. A. K., Tönjes, M., Hovestadt, V., Albrecht, S., Kool, M., Nantel, A., Konermann, C., Lindroth, A., Jäger, N., Rausch, T., Ryzhova, M., ... Jabado, N. (2012). Driver mutations in histone H3.3 and chromatin remodelling genes in paediatric glioblastoma. *Nature*, 482(7384), 226–231. <https://doi.org/10.1038/nature10833>
- Singh, D., Febbo, P. G., Ross, K., Jackson, D. G., Manola, J., Ladd, C., Tamayo, P., Renshaw, A. A., D'Amico, A. V., Richie, J. P., Lander, E. S., Loda, M., Kantoff, P. W., Golub, T. R., & Sellers, W. R. (2002). Gene expression correlates of clinical prostate cancer behavior. *Cancer Cell*, 1(2), 203–209. [https://doi.org/10.1016/s1535-6108\(02\)00030-2](https://doi.org/10.1016/s1535-6108(02)00030-2)
- Tate, M. C., Lindquist, R. A., Nguyen, T., Sanai, N., Barkovich, A. J., Huang, E. J., Rowitch, D. H., & Alvarez-Buylla, A. (2015). Postnatal growth of the human pons: A morphometric and immunohistochemical analysis. *The Journal of Comparative Neurology*, 523(3), 449–462. <https://doi.org/10.1002/cne.23690>
- Wagner, S., Benesch, M., Berthold, F., Gnekow, A. K., Rutkowski, S., Sträter, R., Warmuth-Metz, M., Kortmann, R. D., Pietsch, T., & Wolff, J. E. (2006). Secondary dissemination in children with high-grade malignant gliomas and diffuse intrinsic pontine gliomas. *British Journal of Cancer*, 95(8), 991–997. <https://doi.org/10.1038/sj.bjc.6603402>
- Walker, A. S., Goings, G. E., Kim, Y., Miller, R. J., Chenn, A., & Szele, F. G. (2010). Nestin reporter transgene labels multiple central nervous system precursor cells. *Neural Plasticity*, 2010, 894374. <https://doi.org/10.1155/2010/894374>
- Westermarck, B., Heldin, C. H., & Nistér, M. (1995). Platelet-derived growth factor in human glioma. *Glia*, 15(3), 257–263. <https://doi.org/10.1002/glia.440150307>
- Wu, G., Broniscer, A., McEachron, T. A., Lu, C., Paugh, B. S., Becksfort, J., Qu, C., Ding, L., Huether, R., Parker, M., Zhang, J.,



Gajjar, A., Dyer, M. A., Mullighan, C. G., Gilbertson, R. J., Mardis, E. R., Wilson, R. K., Downing, J. R., Ellison, D. W., ... St. Jude Children's Research Hospital-Washington University Pediatric Cancer Genome, P. (2012). Somatic histone H3 alterations in pediatric diffuse intrinsic pontine gliomas and non-brainstem glioblastomas. *Nature Genetics*, 44(3), 251–253. <https://doi.org/10.1038/ng.1102>

#### SUPPORTING INFORMATION

Additional supporting information may be found in the online version of the article at the publisher's website.

**How to cite this article:** Tomita, Y., Shimazu, Y., Somasundaram, A., Tanaka, Y., Takata, N., Ishi, Y., Gadd, S., Hashizume, R., Angione, A., Pinero, G., Hambardzumyan, D., Brat, D. J., Hoeman, C. M., & Becher, O. J. (2022). A novel mouse model of diffuse midline glioma initiated in neonatal oligodendrocyte progenitor cells highlights cell-of-origin dependent effects of H3K27M. *Glia*, 70(9), 1681–1698. <https://doi.org/10.1002/glia.24189>